Investigation to the effects of double anchor plates on GEWI-piles

BACHELOR THESIS CIVIL ENGINEERING

UNIVERSITY OF TWENTE.

anteagroup

Kolkman T.T.M.

Anselmucci F.A.R.

Scholten N.

University of Twente, Department of Engineering Technology

Antea-Group

10-07-2024

Author

Thomas Teun Merlijn Kolkman
t.t.m.kolkman@student.utwente.nl
Bachelor Civil Engineering

University of Twente
Floriana A.R. Anselmucci

Drienerlolaan 5
7522 NB Enschede
 +31 53 489 9111

Antea Group
Nick Scholten

Zutphenseweg 31-D
7418 AH Deventer
+31 0570 679 44

UNIVERSITY
OF TWENTE.

anteagroup

Abstract

In the world of construction foundations are a core element of structural engineering. As today's society strives to optimal sustainability developments are made every possibility that occurs. A big missed opportunity in the construction field is in the material use in underwater concrete floors. Underwater foundations are held by anchors. These foundations initially experience a lot of upward force due to waterpressure and later experience a lot of downward forces due to loads of the structure. Therefore the anchors need to be resilient against both tensile and compressive forces. To be strong enough, sufficient spacing between the anchor and the flooredge should be applied. Consequently these floors become very thick and use up loads of concrete. This problem can easily be solved by implementing a double anchorage. This research paper looks into the effects of double anchor plates on GEWI-piles on punching shear. GEWI-piles are used for foundation of among others underwater concrete floors. The paper answers how double anchors improve the punching capacity at different floor thicknesses and/or how much the thickness of the floor can be reduced while remaining equal/similar punching capacity. The punching capacity is tested on the stress over the area around the anchors. The model used in this research is based on a segment of a bus underpass that is currently being built in Groningen. The results concluded that a double anchor at equal floor thickness experiences about half the stress levels. When remaining similar punching capacity, the thickness of an underwater concrete floor can be reduced by 20% percent by using a double anchor rather than a single anchor.

UNIVERSITY
OF TWENTE.

anteagroup

Preface

This thesis report is the final product of my bachelor thesis research 'Investigation to the effects of double anchor plates on GEWI-piles'. This thesis is part of my graduation for the bachelor Civil Engineering at the University of Twente. The research is contracted by and performed at Antea Group during a 12 week programme.

Executing this research at Antea Group has introduced me to the corporate sector of civil engineering, although I have mainly performed my own research individually, I do have a better understanding of how such an engineering/consultancy firm operates and the scale and timeline of infrastructure projects. I would like to thank my colleagues at Antea Group for the open welcoming. With thanks in particular to Nick Scholten who was my supervisor at Antea Group and who guided me through the research and helped me answer any questions regarding the research.

Further I would like to thank Floriana Anselmucci, who was my supervisor from the University of Twente. She gave guidance through the research period and the period leading up to the research. Without my supervisors I would not have been able to carry out the research as well.

If you are left with any questions or wish to speak about the research feel free to contact me. For now I hope you will enjoy reading this paper.

Sincerely,

Thomas Kolkman
Deventer, July 2024

UNIVERSITY
OF TWENTE.

anteagroup

Table of Contents

UNIVERSITY
OF TWENTE.

anteagroup

IV

UNIVERSITY
OF TWENTE.

anteagroup

List of symbols & abbreviations

Symbols	Description	unit
d_{eff}	Effective height of the floor reduced by all tolerances	mm
f_{ck}	Design value of the cylinder compressive strength of concrete after 28 days	MPa or N/mm^2
GHG	average high ground water table, (Gemiddeld Hoogste Grondwaterstand)	-
GLG	average low ground water table, (Gemiddeld Laagste Grondwaterstand)	-
h_{avg}	Average floor thickness	mm
NAP	Normal water level in Amsterdam, (Normaal Amsterdams Peil)	m
p	Distance between upper surface of the floor and bottom of anchor disk	mm
p_{max}	Maximum distance of P	mm
p_{min}	Minimum distance of P	mm
tol	Tolerance, deviation of the actual elevation of foundation slab to the theoretical elevation	mm
tol_{anchor}	Tolerance of the anchor's elevation	mm
tol_{bottom}	Tolerance on the bottom side of the concrete slab	mm
tol_{upper}	Tolerance on the upper side of the concrete slab	mm
u_0	Perimeter of anchor plate	mm
u_1	(First) control perimeter	mm
UWC	Underwater concrete	-
V_{Ed}	(Net) compressive/tensile force on anchor	N
v_{Ed}	Shear/punch stress	N
v_{rd}	Shear force or punching capacity/resistance for unreinforced concrete regarding the ultimate limit state	N
β	Reliability index	-

1 Introduction

Proper foundation is essential in the field of construction since otherwise structures cannot be built or will not be stable. Variety of soil and structure properties call for diverse foundations, from shallow to deep foundations. One example of a deep foundation type is a micropiled raft foundation. GEWI piles fall under the category of micropiles and are often combined with a raft foundation (H.G. Kempfert, 2013). These are used when the soil conditions are such that the water table lies higher than the base of a structure and the soil moisture content is regularly high. Foundations like this can be found at structures like basements or tunnels. (Alessandro Flora, 2018)

This research is emphasized on GEWI piles, which name comes from the German word; 'gewinde stab', meaning threaded rod. GEWI piles are made of a composite of materials, which will be discussed in more detail later, and falls beneath a peculiar type of piles called micropiles. Conditions for micropiles are drilled piles with a diameter of less than 300 mm or displacement piles with a diameter no more than 150 mm. Micropiles are often shorter in length and applied to 'raft' or 'floating' foundations. (Hans-Georg Kempfert, 2006)

Due to the high-water content in the soil the soil acts a force upon the raft foundation pushing the entire structure upwards. To counteract this uplift and prevent the structure from drifting, emersion or tilting, the GEWI micropiles pull the foundation down using shear force against the surrounding soil (Hans-Georg Kempfert, 2006). Besides upward forces, from the water pressure, the foundation also experiences downward forces from loads originating from the above structure. The GEWI micropiles should therefore be resistant against both tensile and compressive forces.

GEWI piles are connected to the concrete raft foundation with an anchor plate, see Figure 1A and B for an exposed and a schematic anchor plate. The anchor plate distributes the tension or compression force to the lower and upper surface of the concrete slab in a conical shape, it is therefore crucial to allow an adequately thick foundation to account for proper force distribution, and to avoid exceeding the punching capacity of the concrete.
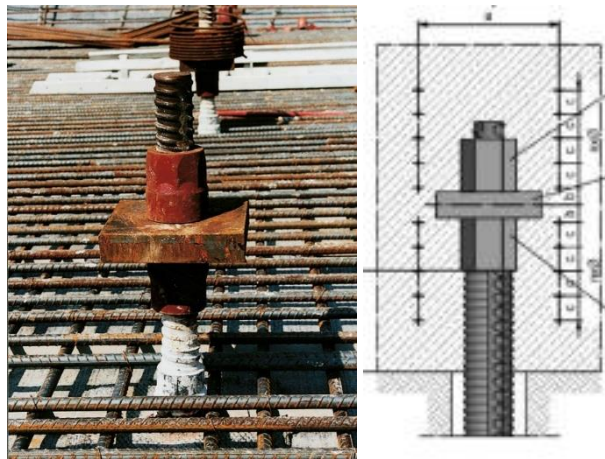
Figure 1: A) Exposed GEWI anchor plate (DYWIDAG, 2024); B) Schematic GEWI anchor plate (DYWIDAG, 2021)

This research paper will focus on the structural effects of the force distribution when a double anchor per pile is applied rather than a single anchor per pile. To ultimately improve force distribution, therefore lower shear stress or reduce material use. The research will be performed by simulating a model in SCIA Engineer. The model will be based upon a tunnel segment of the Bus station tunnel in Groningen which is a completed project executed by Antea Group.

2 Problem Context

2.1 Current state of affairs

In the current state GEWI piles are utilized in an extensive quantity of projects concerning underwater concrete foundation. According to Dutch regulations only a single plate can be placed in the concrete per pile unless research can sufficiently indicate the effects and safety of multiple bearing plates (NEN, 2015). Often engineering firms (e.g., Antea Group) cannot assign enough time and/or personnel to perform such research as they are dealing with specific timeframe and budget. There are some projects in the Netherlands that already have realized the use of a double anchor plate in an underwater concrete foundation. Both the Albert Cuyp and Marnix parking garage in Amsterdam have implemented double anchor plates. (Stephan van Tilburg, 2021) (Arno Poels, 2022) However these double anchors are divided and placed in two separate floors; an underwater concrete floor and a regular floor.

Figure 2A-G show schematic illustrations of the current situation and explain why this regulation is a problem. Figure 2 shows a schematic overview and a legend of the GEWI anchors. The blue arrows in Figure 2A represent the upward force that saturated soil could perform on the concrete due to water pressure. The piles counteract these forces due to the shear friction they exert on the surrounding soil (red arrows). The friction (or downward/tensile force) travels through the rod to the GEWI anchor plate. The anchor transfers these forces onto the concrete, this force transfers according to a conical shape (represented as dotted lines) making the area over which the force is distributed larger than the anchor's area. It is clear that the elevation of these anchor plates in the floor is responsible for the distribution area. This means it is ideal to place the anchor plates furthest from the surface it will exert forces upon, as this will spread the forces over the largest amount of area.

Unfortunately, it is not as easy as placing this anchor higher up in the concrete. Since there are also structural loads (purple arrows) directed in the opposite way (Figure 2B&C), these forces are countered mainly by friction with the soil but also depending on the soil through compressive support (green arrows). Therefore placing the anchor plate very high up in the concrete means a great force distribution for tensile/pulling forces but a very weak distribution for compressive/pushing forces, as showcased in Figure 2D.

A double anchor solves the problem of placing an anchor plate close to the surface without either tensile or compressive force distribution cascading (Figure 2E&F).

Due to the regulations the current best method is to place the anchor plate around the middle of the concrete resulting in smaller but equal distribution of force (Figure 2C). This results in a much larger layer of concrete being necessary to achieve a similar force distribution as its complementary double anchor as can be clearly seen in Figure 2G&H.

In conclusion there is currently an opportunity being wasted that could reduce material use and/or reduce the stress in the UWC due to Dutch regulations.
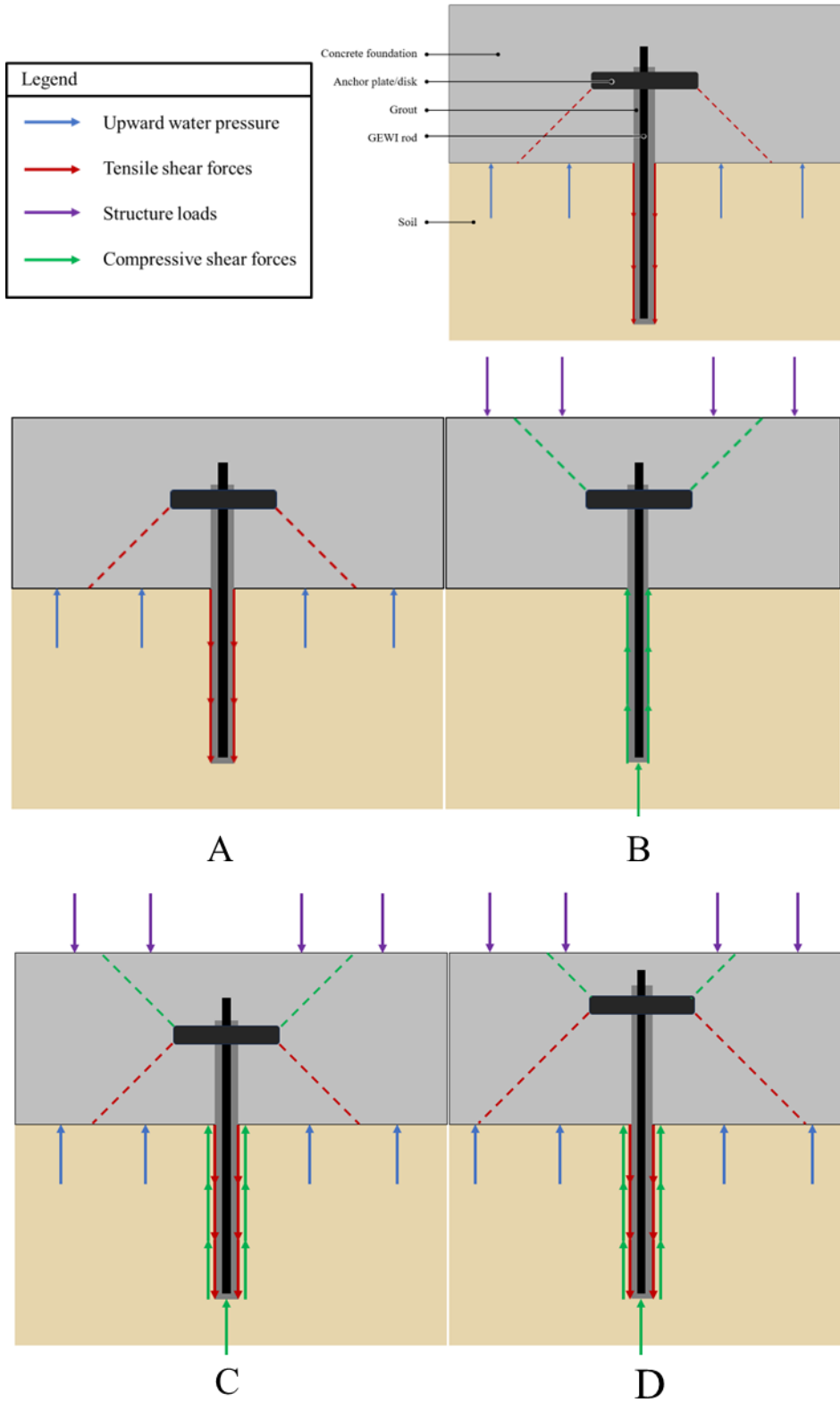
Figure 2: Schematic explanation on force distribution of double vs single anchors
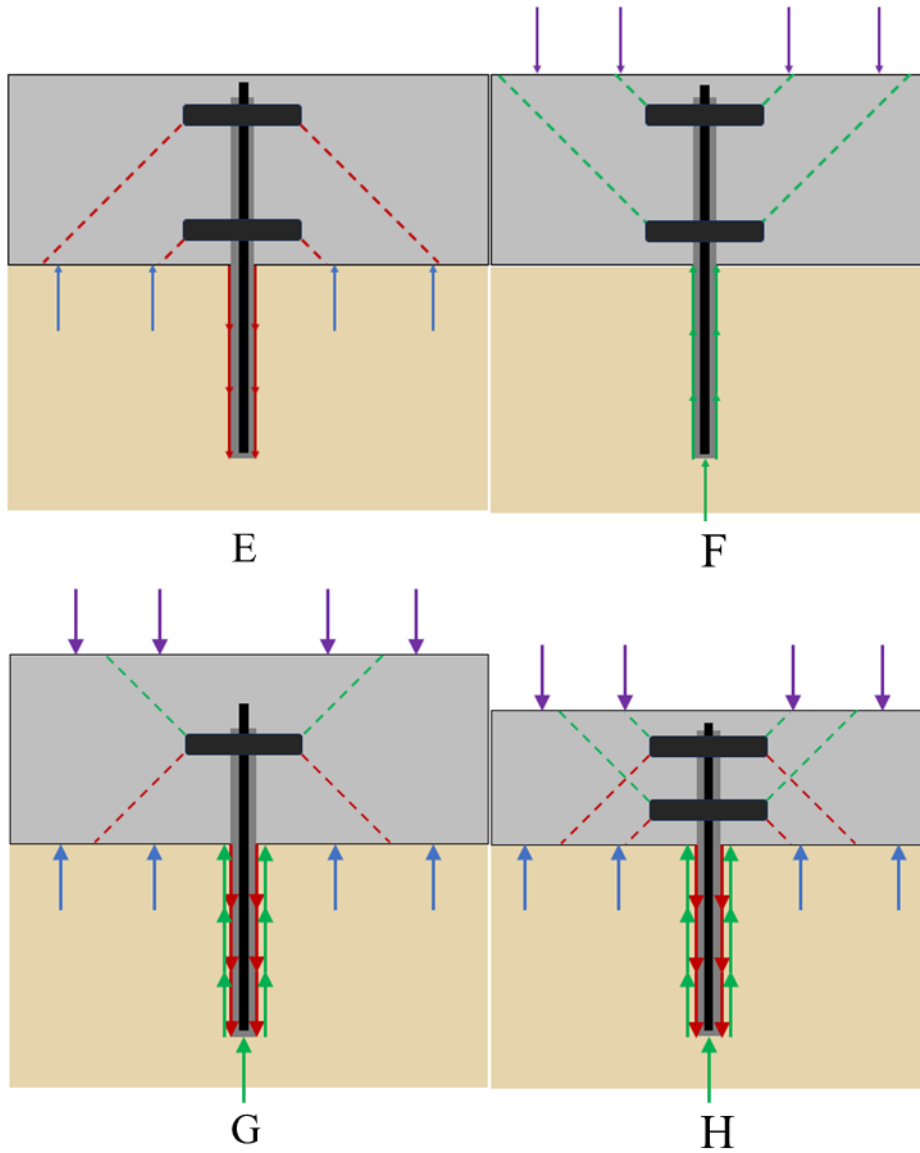
Figure 2: Schematic explanation on force distribution of double vs single anchors

2.2 Relevance

This problem is relevant to the Dutch construction and engineering domain as it has potential for substantial reduction in costs if this different method was allowed without extensive research. Two examples in the Netherlands where this method is already utilized are the Albert Cuyp garage and Marnix garage as mentioned before showing double anchors are feasible. Despite, due to the Dutch construction regulations it is however not allowed to place two of these anchor plates for one rod without elaborate research. The reason for this is that it is not explicitly demonstrable yet what the effect of this modification will be. This thesis will focus on the research of the effects of two plates fixed in the concrete by using a digital model as opposing to the traditionally used single anchor plate per pile.

2.2.1 Involved parties

This research is executed with and under supervision of Antea Group. Antea Group is an engineering and consultancy firm with over 1500 engineers at 5 branches across the Netherlands. The company is active on multiple levels across multiple fields. Tasks as research, design, calculations, organisation and project delivery are subjects Antea Group identifies with. Projects/jobs concepts can vary from construction of bridges, roads to neighbourhood resilience and nature reserves. Antea Group recently finished a project in Groningen, Netherlands, regarding a tunnel underneath the train station. Due to its depth the water foundation was well below the water table making it so upward water pressure was present. Further due to loads of trains running over the foundation experienced load forces. A textbook example were a raft micropiles foundation is suitable. The project made use of GEWI-piles but were forced to apply only a single anchor plate per pile as the Dutch regulations did not permit otherwise. This shows the relevance of this problem to Antea Group but also other engineering firms which might struggle with the same inconveniences.

Other construction and engineering firms in the Netherlands could benefit from this research paper as this paper might kickstart more research in this specific area of foundation. Which ultimately could lead to a change in regulations or help supply information about the subject for investigation regarding their specific projects.

The University Of Twente is also at stake. As it is the originator of this Bachelor Thesis. Besides, the University of Twente assigned a supervisor to audit the progress of the Thesis.

Finally, myself, I am involved and have high stake in this research as it will determine my final grade for my bachelor diploma.

3 Research Questions

Following the introduction the research questions with their correlating sub-questions can now be defined. To reach the desired outcome, it is important to be able to answer the following questions at the end of the research.

> **"What is the effect of a double anchor plate on GEWI-piles on shear punch capacity in an underwater concrete foundation compared to that of a single anchor plate?"**

To be able to answer the main question a few sub questions need to be answered and determined first. Since the research is performed based on the bus tunnel in Groningen it is important to study this case. Therefore the following questions are set up:

A. What are the characteristics and properties of the Groningen tunnel?
   a. Which segment will be selected?
   b. What are the dimensions?
   c. Which forces are active?

Further it is important to establish what results are the objective, and how to achieve those.

B. How will the shear punch capacity be tested/measured?
   a. What formulas are related?

After the main research question is answered , therefore it is known what the effects are of a double anchor plate, the following questions arise.

> **"How beneficial is a double anchor plate on GEWI-piles?"**

With according sub-question:

C. What is the ideal/recommended positioning of the double anchor?"

At the

4 Theoretical background

This chapter will supply background information about underwater pile foundations and the GEWI-anchors more specifically. First the different conditions where pile foundations are often found will be discussed. Next several types of piles will be briefly described and what type GEWI piles fall under. Then an explanation of the structure and the functioning of a GEWI pile is provided.

4.1 Pile foundation conditions

A much-used method of foundation is a foundation based on piles, usually foundations of this type are more expensive due to the depth of the operation. Despite, pile foundations are necessary for a number of cases usually associated to inadequate strength and stability of the soil. The different soil conditions which require pile foundations are listed below.

1. In case the upper soil is too fragile to withstand the compressive forces exerted by the structure above. The piles are connected to a deeper lying bedrock layer to which the piles can transmit the compressive forces to (Figure 3a). Though not always a hard rock layer is present within close distance. In these cases, the piles will transmit the forces to the surrounding soil gradually using mostly friction forces acting between the piles outer layer and the soil as can be seen in Figure 3b.

2. Another reason to implement piles is when horizontal forces are exerted on the above structure. These horizontal forces are wind or earthquakes for example. The piles resist these forces by bending. Horizontal forces are mostly submitted to tall buildings or earth-retaining structures, see Figure 3c.

3. In case the soil is either expandable or collapsible piles will be used. The soil is heavily influenced by the water content, shrinking or expanding of the soil is result of the moisture content decreasing or increasing. Some soil types drastically lose structural stability under high water content risking collapse or damage with other foundations. Piles are drilled to connect to deeper more stable soil, deeper layers of soil fluctuate considerably less in water content giving them more stability (Figure 3d).

4. A fourth reason to install a pile foundation is when the foundation locates below the water table. The high-water content could create uplifting forces which will act on the above structure. In this case the piles will be used to counteract these upward forces as demonstrated in Figure 3e.

5. The last situation where piles are often used is for structures close to open waters where a shallow foundation could fail as a result of soil erosion around at the surface of the structure, see Figure 3f. The piles are extended to levels where erosion will not occur in the foreseeable future. (Das, 2011) (Alessandro Flora, 2018)

This study is focussed on underwater foundations; thus the foundation is located below the water table, situation four therefore applies to this study.
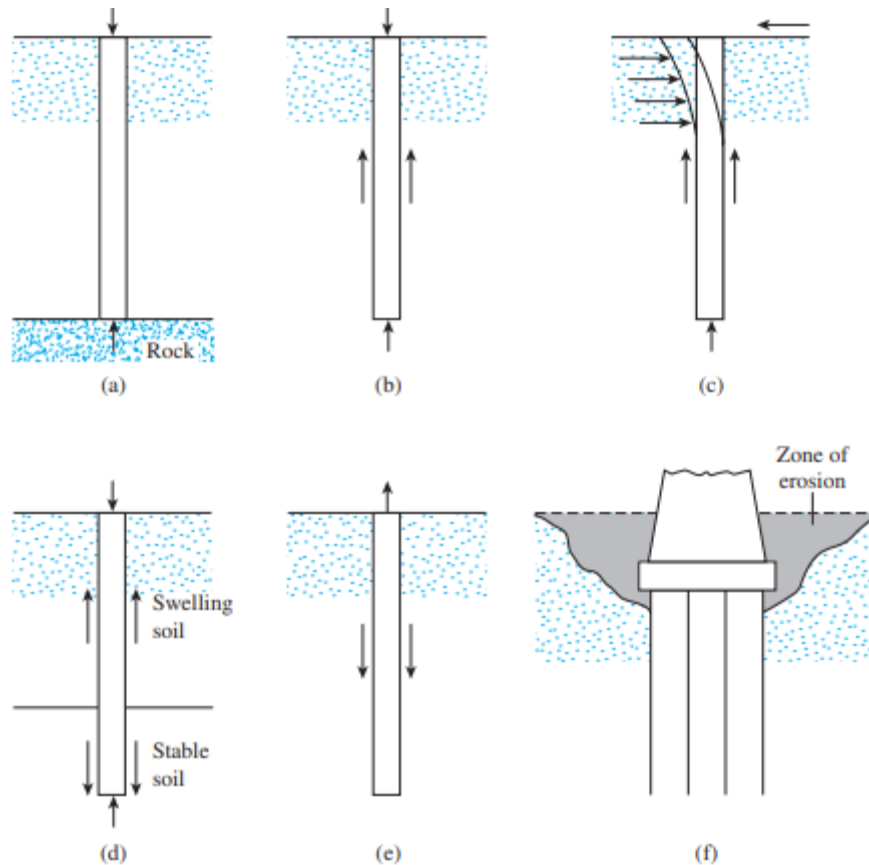
Figure 3: Situations that require pile foundations (Das, 2011)

4.2 Types of piles

The type of pile used for a foundation is dependent on the soil conditions, bearing loads, available space but also economic factors. Some basic examples of pile types are steel piles, timber piles, concrete piles. While steel piles are strong and elastic, easily extendable and reinforced their cost is often high and there is risk of corrosion. Timber piles also have high elasticity, are easy to work /handle, and have low cost, and high life span in right conditions. Disadvantages of timber piles are rotting of timber when exposed to air, and they are difficult or impossible to install in dense soils, further they have limited length and load bearing capacities. Finally concrete piles, advantages are its great load bearing capacities, piles can be created for any length desired. Disadvantages include low elasticity, therefore high risk of fracture, difficult to handle. Further the quality of the piles is dependent on the experience of the installation crew, which could be a reliability.

This research is emphasized on GEWI piles, which fall beneath a type of piles called micropiles. As earlier mentioned micropiles are drilled piles with a diameter of less than 300 mm or displacement piles with a diameter no more than 150 mm. These piles are often relatively short in length and applied to raftfoundations. (Hans-Georg Kempfert, 2006)

4.2.1 Types of micropiles

Micropiles divided into four distinct types, the types distinguish themselves by the method of grouting, the types can be seen in Figure 4. Type A solely uses grouting by gravity. Type B makes use of pressure grouting resulting in a thicker bottom. Type C utilizes both gravity and pressure grouting.

The initial grout layer is poured using gravity. Secondary grout is injected at lower parts through tubes under pressure this is done before the primary grout is dried. Finally type D is similar to type C where it also uses both gravity and pressure grouting. The difference between the two is the secondary grout for type D is only injected once the initial grout is hardened. Further type D can apply post grouting multiple times. (Paul J. Sabatini, 2005)
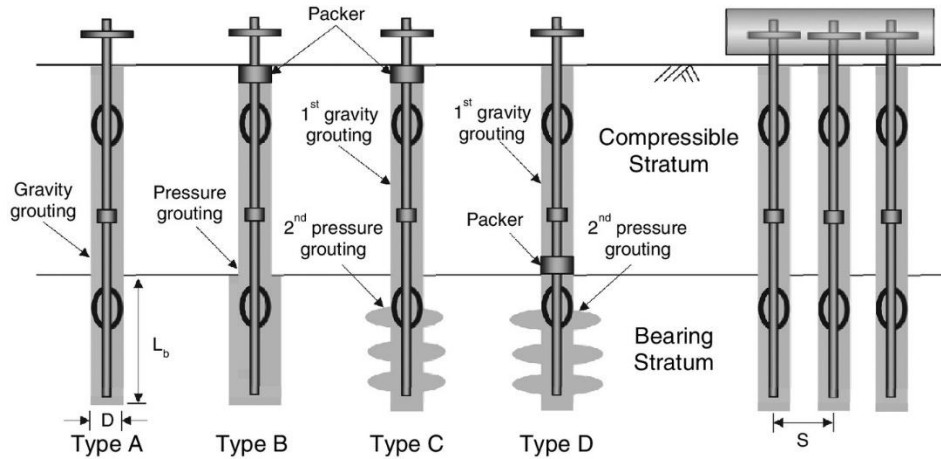
Figure 4: Micropile types A-D (Doohyun Kyung, 2017)

4.3 Structure and functioning of GEWI piles

This section will focus on the description of the structure and properties of GEWI piles as well as the physical functioning of these piles. GEWI piles exist of a heavily threaded reinforced steel bar surrounded by grout. The steel rods have a diameter between 20 to 50 mm. Steel rods are used for their tensile strength properties which are helpful in withstanding and transferring the tensile forces to the surrounding soil created by the water table. The total diameter of the rods and grout layer is a maximum of 300 mm (NEN, 2015). The grout layer serves multiple purposes:

- It is used to exert pressure on the surrounding soil to increase the skin friction.
- Further it acts as a protective layer against corrosion. The cement mortar restrains moisture to encounter the rod disallowing corrosion.

Figure 5 (left) shows a regular GEWI pile. In case this grout layer cannot sufficiently protect the rod from aggressive soil or groundwater an additional protection cover can be applied, named double corrosion protection. Double corrosion protection is achieved by an additional grout layer around the threaded rod, next a plastic corrugated sheathing is installed that surrounds the inner grout layer, Figure 5 (right) shows the Double corrosion protection on a GEWI pile. The double protection is manufactured at the factory. Figure 6 displays the top view of such a double corrosion protection rod. Spacers are placed on the bar which will help centralize the rod in the installation process. Mainly two different types of anchorages are used on the GEWI-poles, plate anchorage which is used for compressive forces and end anchorages which are used for tension. Another feature of the GEWI piles can be equipped with is a post grouting system. This makes it possible to pour grout around the rod after the installation is complete. This would be done to fill up cracks that may have formed and/or to increase skin fraction. (DYWIDAG-Systems International GmbH, 2021)
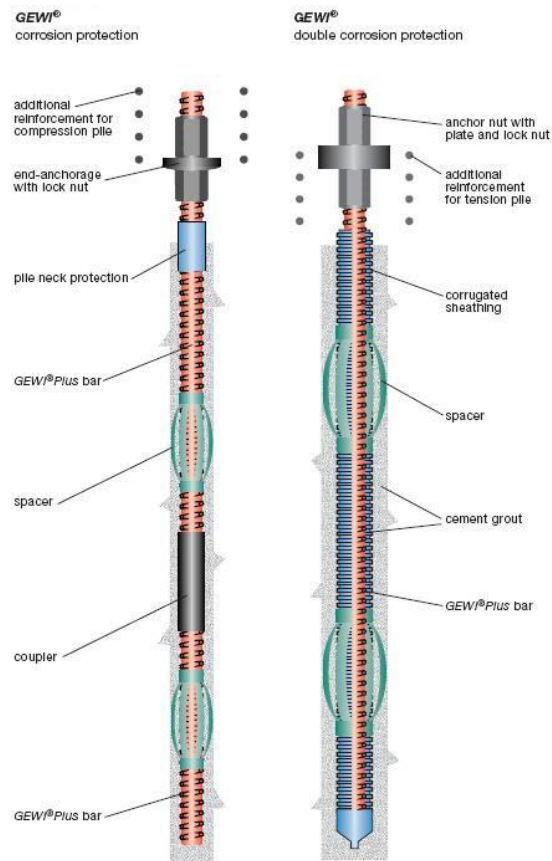
Figure 5: GEWI piles single (left) and double (right) corrosion protection (DYWIDAG-Systems International GmbH, 2021)
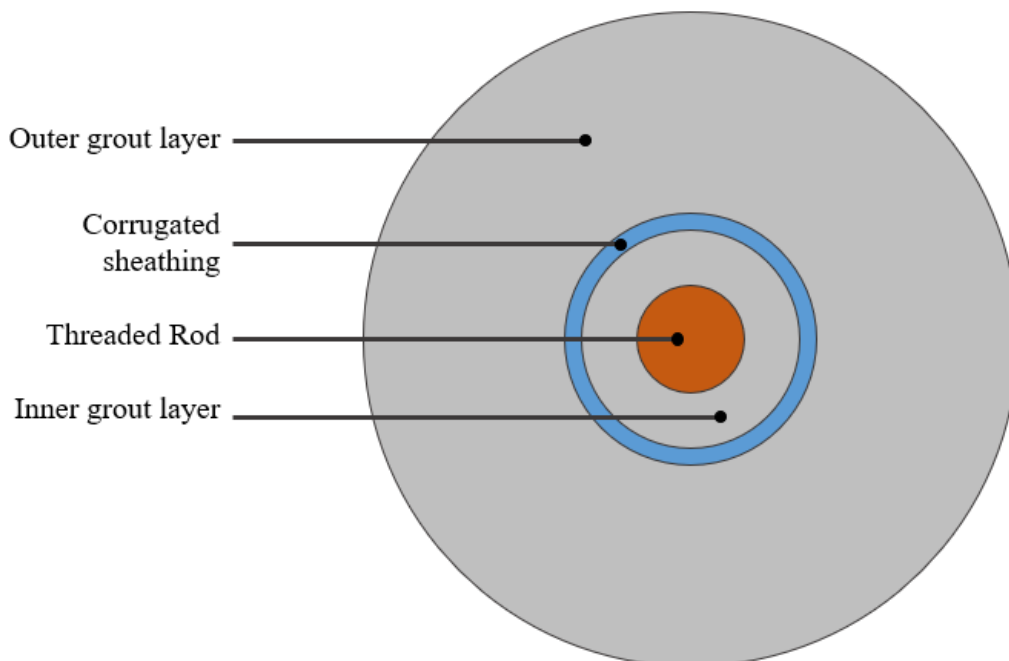
Figure 6: Double corrosion protection top view

To install GEWI piles, first a hole will be drilled often utilizing wash boring techniques. As previously mentioned for double corrosion protection piles the inner grout layer and corrugated sheathing is

preinstalled at the factory. The threaded GEWI rod (with or without double protection) is inserted in the borehole and centralized with the help of spacers. Next the cement-mortar grout is pumped in the borehole from the bottom up.

4.4 Acting forces

One of the most prominent situations when GEWI piles are used is when the foundation is located below the water table. Therefore, the soil is mostly saturated causing uplifting forces on the foundation. To counteract these forces the GEWI piles are installed. The piles are attached to the foundation with an Anchor plate or disk. When the saturated soil performs upward pressure on the bottom of the foundation the GEWI pile resist the force by skin friction against the surrounding soil, pulling/holding the foundation down. This downward force is transferred from the rod to the anchor plate, which then pushes down on the concrete foundation as shown in Figure 7. The downward force exerted by the anchor plate on the foundation is transmitted in a conical shape distributing the force over a larger area than the one of the anchor disk itself. Consequently, increasing the distance between the anchor plate and the foundation's surface will increase the distribution area, lowering the stress. As showcased in Figure 7 the anchor plate is shifted upwards, resulting in an increased force distribution for tensile forces. Though GEWI piles are not exclusively used for tension, often the forces working on these piles alternate between tension (red) caused by upward water pressure (blue) and compression (green) caused by structural loads (purple). Shifting the anchor plate higher up in the foundation as is done previously in Figure 7, results in shorter distance between the anchor plate and the foundation's upper surface. Reducing the distribution area in this direction, increasing stress during compression.
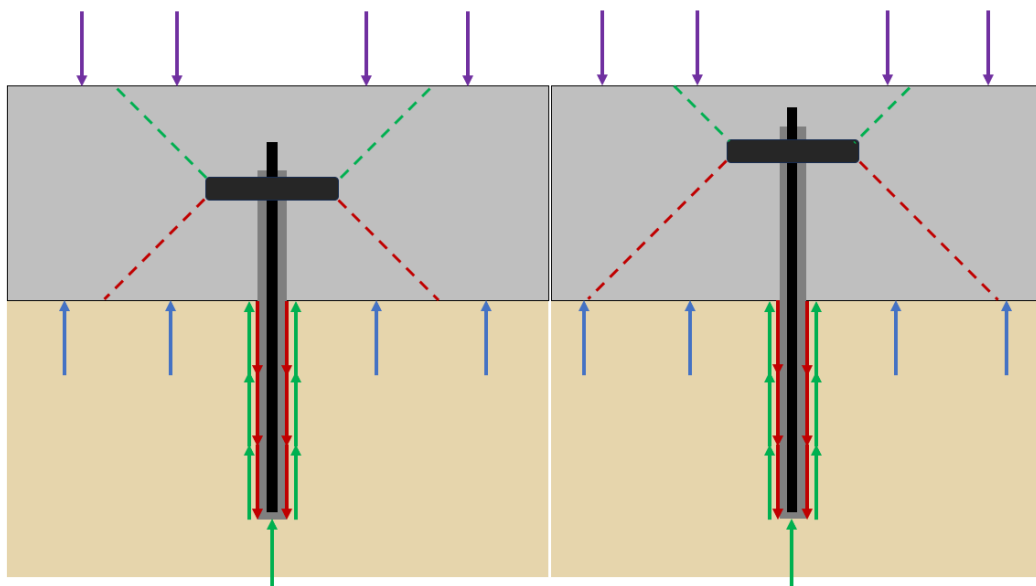
Figure 7: Shifting singular anchor higher up

As before mentioned the forces of the anchor plates onto the concrete foundation distribute in a conical shape. According to European construction code NEN-EN 1992-1-1 the angle of this cone shape can be defined as is done in Figure 8. The angle is determined by the ratio of height to width/radius of the first control perimeter u_1. The width/radius is defined as twice the effective height

(d), the effective height is the total height of the plate (h) minus the diameters of reinforcements and their tolerance/spacing.[1] This gives an angle of $\tan^{-1}(1d/2d) \approx 26.6°$. (NEN, 2011)
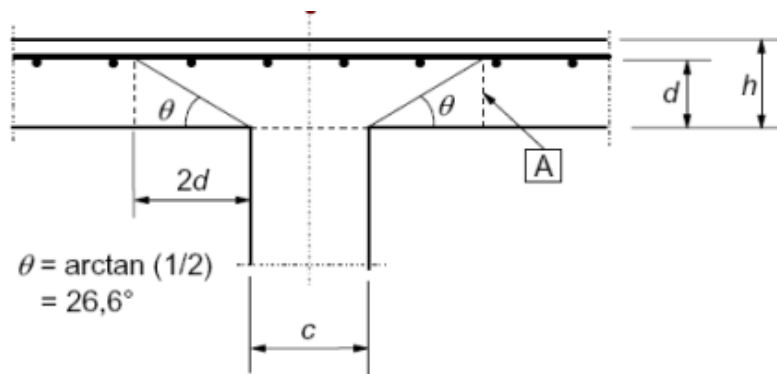
Figure 8: Anchor force distribution (NEN, 2011)

4.5 Punch test

The connection between an anchor disk and the underwater concrete foundation should be tested on and satisfy piercing limits. To test the resistance of the concrete to punching two components are necessary: the punching/shear stress (v_{Ed}) of the anchor and the punching/shear resistance ($v_{Rd,c}$) of the concrete foundation. To pass the test the shear stress must strictly be less than the shear capacity, $v_{Ed} \leq v_{Rd,c}$. (NEN, 2011)

4.5.1 Shear stress

First, the calculation method for determining the punch/shear stress will be discussed. The standard equation for shear stress v_{Ed} is:

$$v_{Ed} \quad = \beta * \frac{V_{Ed}}{u_i d} \qquad \qquad \textbf{Eq. 1}$$

Where:

d   is the effective height of the plate, for which the next equation can be taken.

$$d_{eff} \quad = \frac{(d_y + d_z)}{2} \qquad \qquad \textbf{Eq. 2}$$

d_y, d_z is the effective height in the y- and z- direction of the control cross section;
u_i is the length of the control perimeter.;
V_{ed} is the net force working on the pile;
β   is determined according to the following suggestion:

---

[1] Note that in this Figure 8, the effective height d is taken from the bottom of the floor (where the column meets the floor). In this research the effective height will be taken from the connection to the floor, the anchor, which is more located towards the middle of the floor. This does not change the ratio/angle of the conical shaped force distribution.
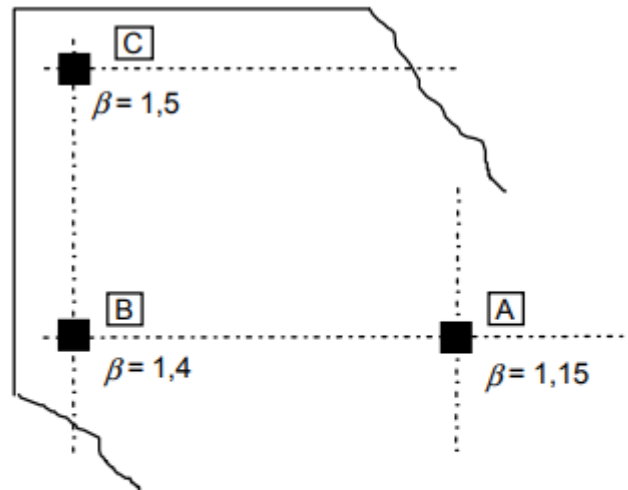
Verklaring

A	middenkolom
B	randkolom
C	hoekkolom

Figure 9: Recommended values for β (NEN, 2011)

In Figure 9 the values of β are defined by the respective position of the anchor/pile in the plate. Three possibilities concern A. middle/internal column, B. edge column, and C. corner column. SCIA Engineer applies the different factor values according to their relative position in the structure. (NEN, 2011). Figure 10 shows the initial control perimeter u_1 of anchors at the three respective locations.
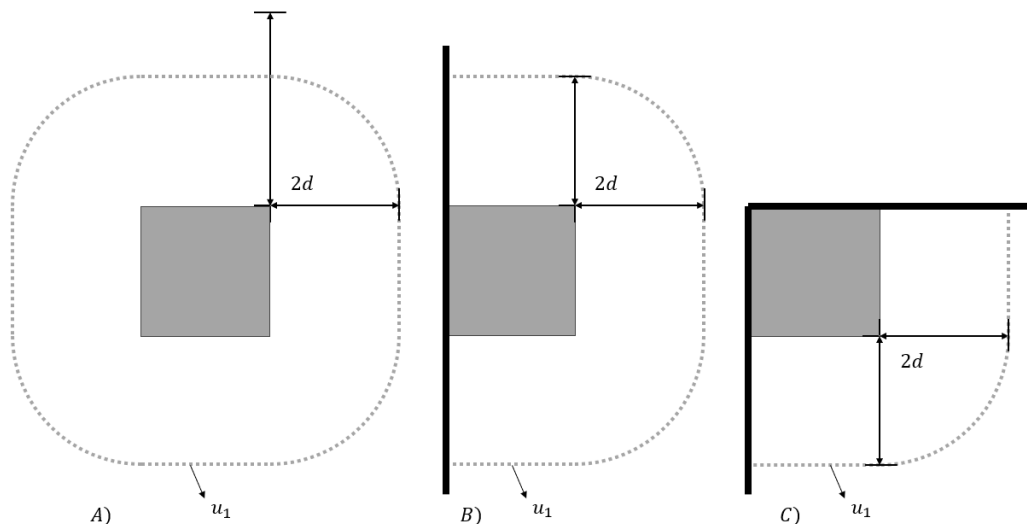
Figure 10: Initial control perimeters u_i around stressed areas for A) middle, B) edge, C) corner anchor

UNIVERSITY OF TWENTE.

anteagroup

4.5.2 Shear capacity

The next set of equations will describe the punch capacity (V$_{Rd}$) of the unreinforced underwater concrete.

$$v_{rd} = [C_{Rd,c} * k(100\, \rho_l\, f_{ck})^{\frac{1}{3}} + k_1 \sigma_{cp}] * b_w * d \qquad \text{Eq. 3}$$

Where:

$C_{Rd,c}$ = $0.18/\gamma_c$

γ_c = 1.5

f_{ck} Is in MPa

k = $1 + \sqrt{200/d_{min}} \leq 2.0$

ρ_l = $\dfrac{A_{sl}}{b_w d} \leq 0.02$

A_{sl} Is the cross sectional area of the tensile reinforcement bars

b_w Is the smallest breadth of the cross section of the tensile zone

k_1 = 0.15

σ_{cp} = $\dfrac{N_{ed}}{A_c} < 0.2\, f_{cd}\ (MPa)$

N_{ed}

A_c

4.5.3 Anchor elevation

To be able to test on punching the elevation of the anchor disk within the foundation should be appropriate. To determine the extremes of the elevation p the following equation below are used, which are in accordance with the terms described in CUR77.

$$P = P_{min} \leq P \leq P_{max}\ (mm) \qquad \text{Eq. 11}$$

$$P_{min} = tol_{upper} + tol_{anchorage}\ (mm) \qquad \text{Eq. 12}$$

$$P_{max} = \frac{h_{gem}}{2}\ (mm) \qquad \text{Eq. 13}$$
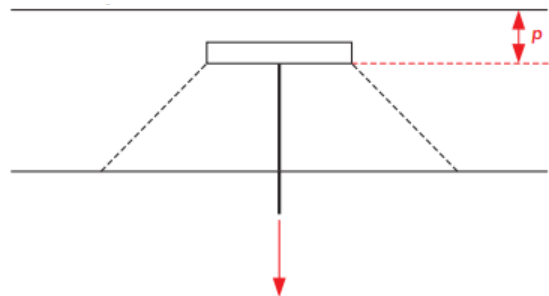
Figure 11: Elevation of anchor (p) in underwater concrete

UNIVERSITY
OF TWENTE.

anteagroup

The tolerance (tol) is the deviation in the floor thickness on the upper and bottom side of the concrete slab (Figure 12). As the concrete foundation is installed under water it must be poured by marine divers with low visibility and hard/limited reach. Further irregularities in the subsoil are hard to spot and mitigate. These are reasons for the high tolerance rates found at underwater concrete foundations.
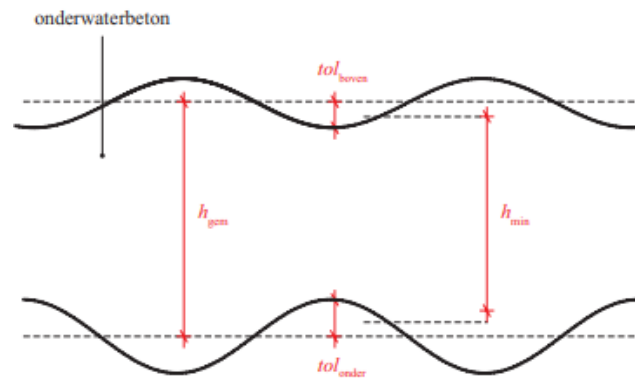
Figure 12: Foundation slab showing avg height and tolerances (deviations)

Tolerance for the bottom surface (tol$_{bottom}$) is determined by the subsoil, possible filling layer. For clay soils it is usual to implement a sand/gravel filling layer (circa 500 mm) for peat soils this is even mandatory. This filling layer improves the stability, decreases the tolerances and it helps cleaning the construction pit. Consequently, the recommended tolerances for the bottom are:

- 150 mm for sand/gravel soils
- 350 mm for clay soils
- 150 mm for soils where filling layers are applied

The tolerance for the upper surface of the foundation is determined by the pouring method. The tolerance values are subsequently:

- 75 mm for the Hop-dobber-method
- 150 mm for the Contractor- and Ventiel-method

Further there is the tolerance for the anchor plate describing the deviation of the elevation of the plate in the concrete layer. This tolerance is determined by the inserting method of the anchors. The CUR77 recommendations follow:

- 100 mm for anchorages on a single level
- 100 mm for encasing of diaphragm wall

Now that the tolerances are established the P$_{min}$ can be determined.

$$P_{min} = tol_{upper} + tol_{anchorage} \; (mm)$$

$$P_{min,up} = 75 + 100 = 175 \; (mm)$$

$$P_{min,bot} = 150 + 100 = 250 \; (mm)$$

Eq. 12

5 Case study

As mentioned before the parameters, variables, conditions, structure specifics will be based on the bus underpass in Groningen. First some background information about the case will be given, how it's design consists of multiple different sections and which section will be the inspiration for this research.

The case that will be used in this research is the Groningen bus underpass Project. Project specifics and environment conditions will be directly drawn from the case. The Groningen bus underpass is a project adopted by Antea Group commissioned by Strukton Rail. The 270 m underpass connects the new bus parking area at the Southsquare with the Norhtern side of the Station (Figure 13). Hereby it crosses 4 traintracks, a cycling lane and a vegetation strip. The underpass is divided into 11 segments. Segments 1, 2, 8-11 are open segments. Segments 3-5 are pergola segments which are overarched by the vegetation strip. Segment 6 is the train track segment which is below the 4 train tracks. Thus experiences additional loads as a result of the train traffic. Segment 7 is the basement segment which is the lowest/deepest segment thanks to the pump basement/technical room.
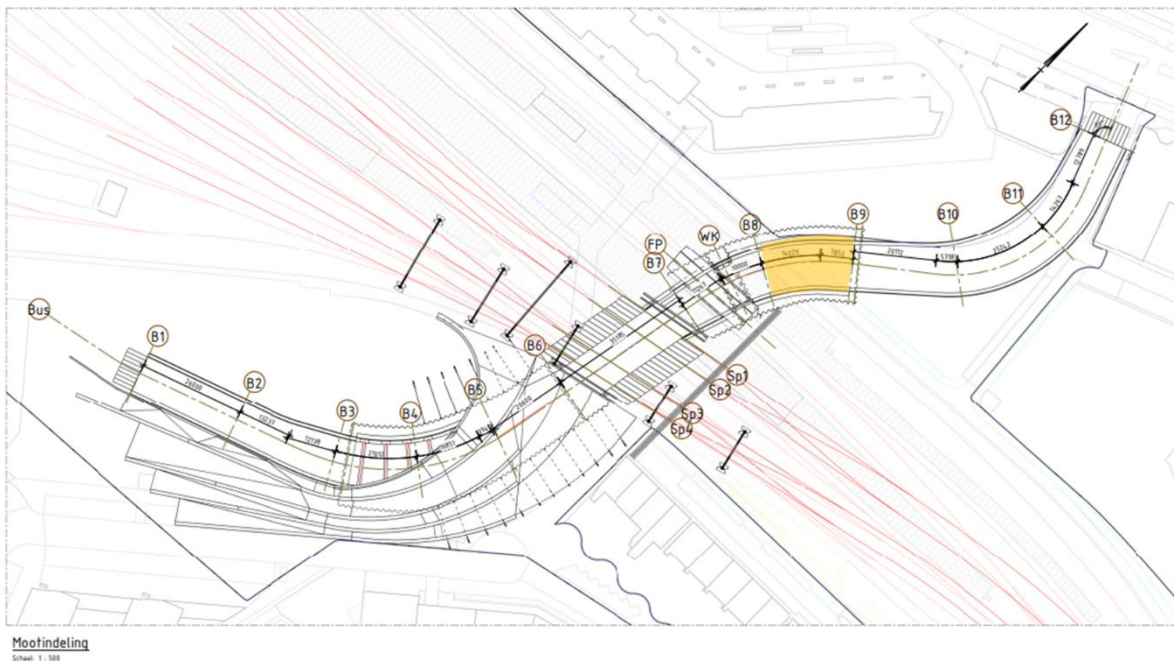
Figure 13: Overview of tunnel segments

To keep the modelling feasible the segments with excessive complications, Pergola segments (3-5), Track segment (6) and Basement Segment (7) are eliminated. The attendant complications are irrelevant to the research and therefore unnecessary to include. Therefore a segment from the Open Segment class will be selected to base the model upon. The researched is aimed at foundation floors below the water table. This eliminates segment 1, 2, 10 and 11 as all of their floors are not below NAP +/- 0, leaving segments 8 and 9. Segment 8 has, in contrary to 9, an additional underwater concrete floor below the regular foundation floor. For this reason segment 8 (highlighted in Figure 13 & Figure 14) is picked as the leading example for which the research is based upon.

UNIVERSITY OF TWENTE.

anteagroup

5.1 Segment 8

Figure 14 displays segments 7 to 11 and highlights segment 8. With 50 GEWI anchors this segment shares the most anchors along with segment 2 of the open segments. The segment is between 19.440 m and 22.956 m long depending on which side is measured. The segment consists of two concrete floors; a regular floor of h_{avg} = 800 mm thick and an underwater concrete floor of h_{avg} = 1000 mm thick. The floor is angled with the south side as the lowest point at -3.10 m (middle of regular floor) and -1.73 m at the north side, which correlates to an angle of 6.3%. Walls on either side go up to +3.4 m. Technical drawings of the side- front- and top view of segment 8 are provided in Figure 34 to Figure 36 in Appendix 12.1 to give a clearer understanding of the dimensions of the segment.

The specific anchor is of the type GEWI 63.5TR, (diameter of threaded rod: Ø= 63.5 mm). The anchor piles reach a depth of NAP -21.500 m, meaning the piles have a length between 18.370 m and 19.701 m. The anchor plates have dimensions of 350 x 350 mm.
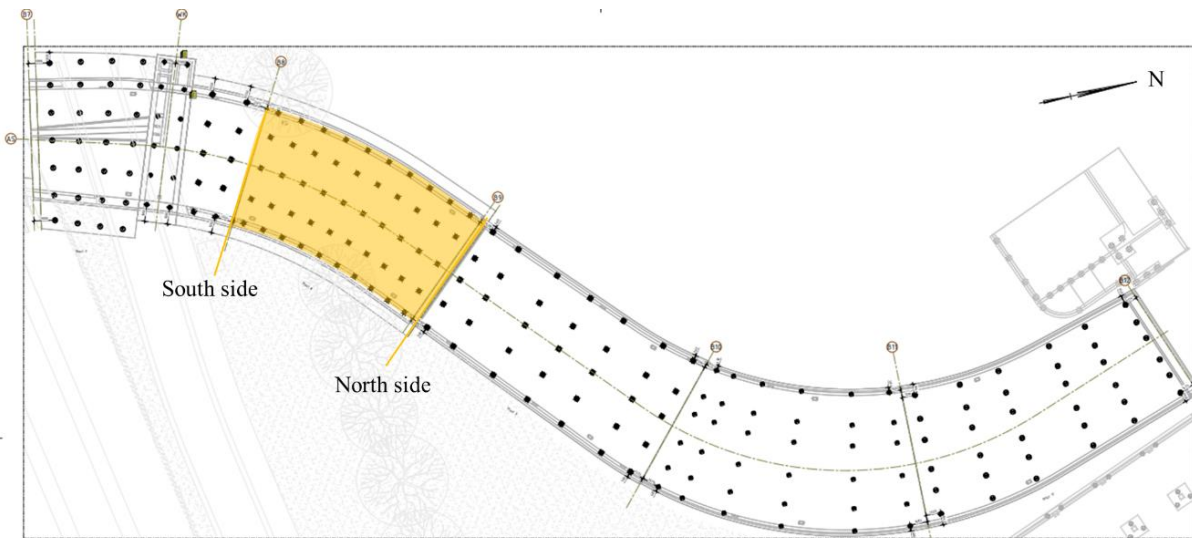
Figure 14: overview of tunnel segments 7-11

5.2 Defining loads

This chapter will discuss all the relevant active loads for tunnel segment 8. It provides all the load values and how these values came to be. The relevant loads are taken from the calculation rapport from the Groningen Bus Underpass, though will be briefly elaborated here to avoid a black box model. Figures of the loads implemented in the model can be found in Appendix 12.2.

5.2.1 Permanent loads
Self-weight

The self-weight of the tunnel segment is generated automatically by the SCIA software. All members placed/built are addressed with a weight according to their volume and density of its' material.

UNIVERSITY
OF TWENTE.

anteagroup

Resting Load

Resting loads are determined by permanent weights that do not perform any bearing, E.G. asphalt. For asphalt a thickness of 0.12 meters is assumed at 23 kN/m^3, resulting in a resting surface load of 0.12 x 23.0 = 2.8 kN/m^3. Further the load of baffle plates and parapets is added in the resting loads these amount to a line load of 14.0 kN on the walls of the segment. (see 12.2.1)

Ground and Water Pressure

The soil surrounding the floor and walls of the underpass perform a permanent load on the structure. This magnitude of the load is dependent on the height of the current watertable. An average minimum and average maximum watertable is established, NAP +0.500 m and NAP +2.500 m respectively, These are considered to calculate the minimum and maximum loads performed by the ground and water of the soil. Both horizontal and vertical loads are taken into account. Further the calculations will be performed for both the North and the South side separately as they are located at different elevations resulting in experiencing different loads.

Ground and Water Pressure North side

The GLG is defined as +0.500 m pertaining to NAP (+/- 0.000 m), while the GHG is defined as +2.500 m. For segment 8, At the north side, the top of the floor is at a level of -1.330 m. The combined horizontal pressure comes down to 62.11 kN/m2 (at -1.730 m NAP), the vertical ground pressure remains 26.3 kN/m2 (at -2.130 m NAP) for GLG. For the high water table (GHG) the loads are a horizontal pressure of 71.42 kN/m^2 and a vertical pressure of 46.30 kN/m^2. (See 12.2.2)

Ground and Water Pressure South side

The GLG (=average low ground water table) is defined as +0.500 m pertaining to NAP (+/- 0.000 m) while the GHG (=average high ground water table) is defined as +2.500 m. The loads at the south side of the segment came down to a combined horizontal pressure of 80.10 kN/m2 (at -3.100 m NAP) and a vertical ground pressure of 40 kN/m2 (at -3.500 m NAP) for GLG. For the high water table (GHG) the loads are a horizontal pressure of 92.11 kN/m^2 and a vertical pressure of 60 kN/m^2. (See 12.2.2) [2]

Swelling Load

Due to excavation of the construction pit swelling occurs in the compressible soil layers. Piles, which are placed prior to excavation experience a reduction mainly in the tensile bearing capacity due to the swelling of the soil. For construction pits utilizing underwater concrete the swelling will convert to an additional upwards load. Though its significance can be neglected when sufficient waiting time is applied.

Shrinking Load

---

[2] Due to limiting abilities in SCIA engineer to perform a punch test on slanted floors. The floor has levelled resulting in equal **horizontal** pressure at the north and south side of the segment, namely 80.10 kN/m^2 for GLG and 92.11 kN/m^2 for GHG. (See 12.2.2)

The shrinking load will be addressed as a temperature load in the model. A predetermined spreadsheet is used to define the temperature load equivalent to the represented shrinking load. As the floor/wall thickness is barely influential for the resulting shrinking load the calculated load can be universally applied to all floors/walls regardless of dimensions. A constant temperature load of -26.60 °C will be implemented as representative of the shrinking load. (See 12.2.3)

5.2.2 Variable loads
Temperature loads

For the temperature loads first a reference temperature is set at T_{ref} = 15 °C. The extreme temperatures are shown in Figure 15 for winter and summer at either side of the concrete slab. In summer the boundary temperatures are +35.0 °C on the inside and +13.0 °C on the groundside. During winter the temperatures fall to -15.0 °C on the inside and +3.0 °C on the groundside.
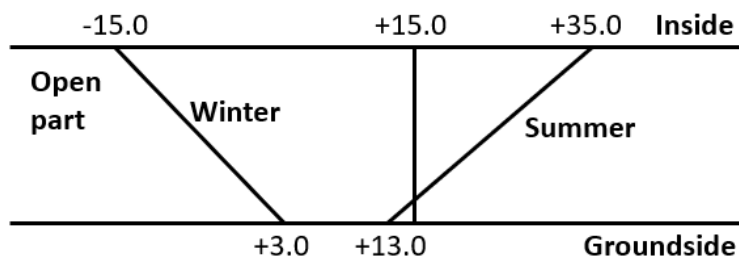
Figure 15: Temperature loads in- and outside

Temperature Load floor

The load that the difference in temperature bears on the floor is determined by the difference of the extreme temperatures with respect to the reference temperature and the maximum and minimum temperature change over 24 hours. The floors temperature difference over 24 h is consistently lower than that for walls due to an additional asphalt paving of 120 mm. Summed up the temperature difference that occurs upon the floor during summer is $\Delta T_{sum,in}$= +24.54 °C and $\Delta T_{sum,gr}$ -3.16 °C. During winter the maximum temperature interchange is $\Delta T_{win,in}$ = -32.22 °C and $\Delta T_{win,gr}$ = -11.43 °C. (See 12.2.4)

Temperature Load walls

Due to different thickness and no additional asphalt paving on the walls the temperature difference for the walls are slightly higher compared to the floor. For summer the maximum temperature change is $\Delta T_{sum,in}$ = +31.17 °C and $\Delta T_{sum,gr}$ = -4.60 °C. For winter the maximum temperature difference is $\Delta T_{win,in}$ = -34.47 °C versus $\Delta T_{win,gr}$ = -10.96 °C. (See 12.2.4)

Ground Level Load

Ground level load will be applied in accordance with Conform ROK 1.4 chapter 10 article 9.4/9.5 and CUR 166 part 1, article 3.3.10. These norms predefine the ground level load to $q_{e,v}$ = 20.0 kN/m². Combined with the neutral ground pressure coefficient of K_0 = 0.5 the final ground level load is equivalent to a surface load of q = 10 kN/m2 on both outside walls. (See 12.2.5)

UNIVERSITY OF TWENTE.

anteagroup

Clamping Load

Deformation caused by temperature fluctuations and changing traffic loads can cause an increased pressure performed by the ground. When the construction expands, the abutments are moving/pushed into the ground increasing the grain pressure. The loads resulting from this deformation is calculated by a predefined spreadsheet. Final loads amount a line load on either outside wall of $F = 5.80$ kN/m on the North side to $F = 6.02$ kN/m on the South side. The load will be implemented as a trapezoid. (See 12.2.6)

Horizontal Traffic Load (Braking)

Traffic will exert loads in vertical direction (gravity) as well as horizontal direction, this is the result of braking. The horizontal braking load is designed in accordance with NEN-EN 1991-2 art. 4.4.1. subsequent $Qe = 0,6$ x $\alpha Q1$ x $Q1k + 0,1$ x $\alpha q1$ x $q1k$ x $w1$ x $L = 428$ kN. Consequently a lineload of $428/22.956 \approx 18.3$ kN/m is implemented on the surface of the concrete floor in the south direction. (See 12.2.7)

Vertical Traffic Load

The traffic through the underpass is solely busses, the model provided/used by Antea Group has distinguished the vertical traffic loads in one surface load across the entire floor surface of 2.5 kN/m^2. And 81 different variations of smaller but more densely packed surface loads covering only parts of the floor's surface. These loads are 2x 58.24 kN/m^2, 2x 116.49 kN/m^2 and 2x 174.73 kN/m^2. The variants of these traffic loads diverge in positioning and location of the smaller surface loads. In the model for this research the general surface load of 2.5 kN/m^2 has been implemented as well as 1 of the variants of the more targeted traffic loads. (See 12.2.8)

5.2.3 Fatiguing loads
Concrete Fatiguing

The concrete experiences fatiguing as a result of the traffic loads. The tunnel is solely being utilized by city busses, exact usage is therefore easily defined and thus used to determine the fatiguing loads. Daily 2200 busses drive through the tunnel in either direction. The technical lifespan should reach 100 years; $n = 2200 * 365 * 100 = 80.3$ million ($8.03 * 10^7$) busses.

5.2.4 Load combinations
As the forces exerted on the structure act concurrently load combinations are made to account for this phenomenon. Temperature and ground/water pressure loads are modelled in two extremes, summer vs winter and low vs high water table, which cannot occur simultaneously. Therefore two load combinations are implemented. High water levels often occur during periods with more precipitation thus during the winter while lower water levels more often occur during drier periods during the summer. Hence the loads of winter temperatures are combined with the loads of high water table and vice versa, the summer temperature loads are combined with the loads of the low water table. Further for both of the load combinations all other loads (non-period related) are included as well.

Figure 16: Load Combinations

5.3 Reinforcement bars

Reinforcement bars are placed in the upper and lower side of the plate. The rebar layout as displayed in Table 1, Table 2 and Figure 17 will be implanted in the concrete floor. The reinforcement layout is copied from the technical report of the tunnel which are determined by calculations performed through automated spreadsheets.

Table 1: Upper and lower latitudinal, and longitudinal rebars

Reinforcement bars segment 8

	Coverage [mm]	Diameter [mm]	Spacing [mm]
Upper side latitudinal direction	65	20	100
Lower side latitudinal direction	60	32/25	200
Longitudinal reinforcement	60	25	100
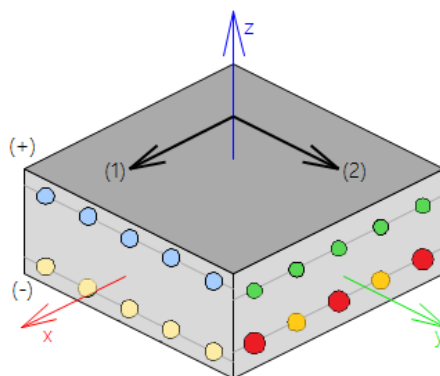
Figure 17: Rebars in the floor

Table 2: Basic rebars and additional rebars colorcoded

layer	Basic Rebars		Additional Rebars	
	Diameter [mm]	Spacing [mm]	Diameter [mm]	Spacing [mm]
1+	25	100	-	-
1-	25	100	-	-
2+	20	100	-	-
2-	32	200	25	200

6 Model

Segment 8 of the bus underpass is modelled in SCIA Engineer. The technical drawings show a curved road piece/tunnel section, in the model this curvature is not taken into account. This would resolve in too many sub wall elements and sub loads, therefore dramatically increasing the labour in constructing the model but also the speed of the calculations/simulations. However the difference in length and anchor distribution is considered. Consequently, the following anchor layout evolves (Figure 18):
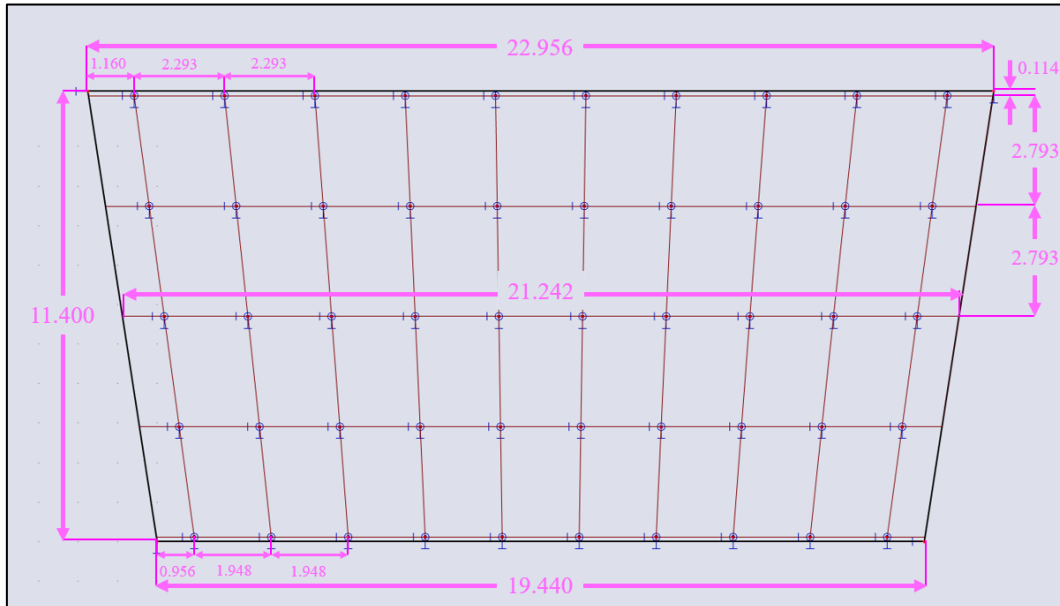
Figure 18: Layout of model dimensions and anchor locations

The model only allows for a single anchor connection per floor. Therefore to facilitate anchors at different elevations within the floor, the floor is divided into two separate subfloors that overlap through each other. Both floors have a thickness of the total floor thickness, a bottom floor with a lower heartline and an upper floor with a higher heartline as shown in Figure 19 (right). The anchors are connected on the heartline, changing the elevation of the heartline changes the position of the anchors. For the control model only a single floor will be used as shown in Figure 19 (left). To compensate for the additional self-weight load carried by the extra floor, the material composition is adapted for these two subfloors to be at half the density (weight) while cherishing other material properties.
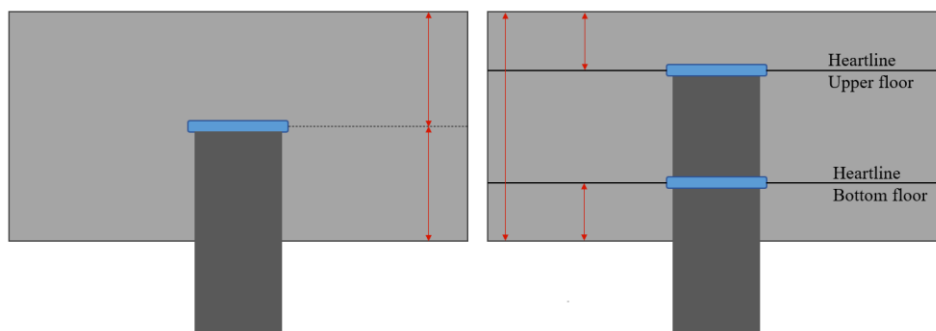
Figure 19: Cross sectional layout of anchors in the floor(s)

Further the slope of the tunnel segment will not be accounted for since SCIA is not able to perform the punch test on sloped/angled plates. This slightly changes the horizontal ground/water load.

UNIVERSITY OF TWENTE.

anteagroup

6.1 Cases

The results will be determined for a multitude of examples, varying in total floor thickness and spacing/elevation of the anchors. Also a distinction is made between an underwater concrete floor and a regular floor. Further the underwater concrete floors are distinguished into right after the initial placement of the underwater concrete floor and when the final construction is done (including the load of/on the walls and traffic loads). As before mentioned in 8.2.4 each case will be simulated for both load combinations; LowWaterSummer and HighWaterWinter. The different cases are shown in Table 3 below where layout A is always the control floor with a singular anchor per pile and layout B-D have floors with two anchors per pile decreasing in floor thickness. In chapter 4.5.3 the minimum spacing/tolerance between the anchor and the floor edge for underwater concrete was defined, namely; $P_{min,up}$ = 175 mm and $P_{min,bot}$ = 250 mm. These boundary values are chosen for the spacing in the UWC floors to attain the largest effective height as possible. Figure 20 shows the cross-sections of layout A-D of the underwater concrete floors including the placement of the anchors.

Table 3: Modeled cases

Layout	Total floor thickness (mm)	Elevation lower anchor w.r.t. bottom of the floor (mm)	Elevation upper anchor w.r.t. bottom of the floor (mm)
Case: Regular Concrete Floor			
A	800	400	-
B	800	150	650
C	600	150	450
D	500	100	400
Case: Underwater Concrete Floor Inintial			
A	1000	500	-
B	1000	250	825
C	800	250	625
D	750	250	575
Case: Underwater Concrete Floor Final			
A	1000	500	-
B	1000	250	825
C	800	250	625
D	750	250	575

Figure 20: Underwater concrete floor Layout A- D in order and their anchor placements

6.2 Anchor points

Section 8 of the underpass has a total of 50 anchors/piles. The model calculates the forces exerting on the floor and the stress around the anchors for each anchor point. Each anchor point is named and addressed individually, the location and name of each anchor is shown in Figure 21 . The research floors however will have two anchors per pile. A total of 100 anchors are counted, 1-50 on the upper heartline/floor and 51-100 on the lower heartline/floor. The upper anchors will only be used for compression while the lower anchors solely exercise tension. Depending on the load combination and case the overall (net) punch force (Ved) per pile will either be compressive (positive) or tensile (negative). The piles do not experience both compressive and tensile forces simultaneously, the absolute values of the net punch force will be taken for the calculation of the stress as a result of the punching shear. Therefore the results will only be shown as anchor points/piles 1-50, though these results do in fact include the stresses as a result of tension through anchor points 51-100. The position of anchors 51-100 are directly beneath anchor points 1-50 respectively.
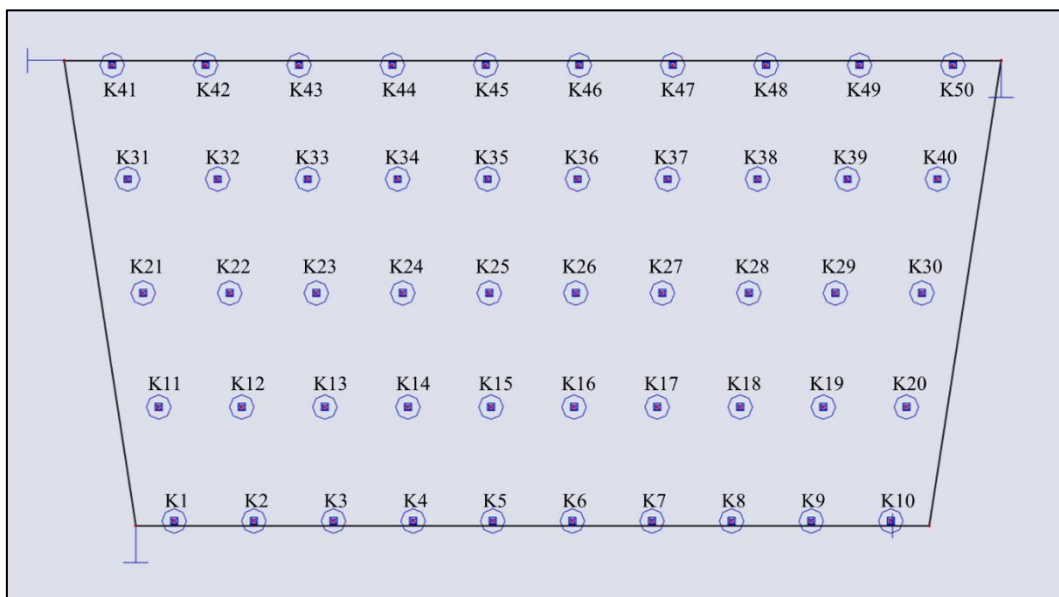
Figure 21: Anchor locations

7 Results

The results in this chapter show the stress levels of the concrete floors around each pile/anchorpoint. The stress is calculated according to the following equation $v_{Ed} = \beta * \frac{V_{Ed}}{u_i d}$ (equation 1, chapter 3).

The stress is measured in MPa for the perimeter u_0 of the anchor plate itself (350x350 mm) and for the first control perimeter u_1 which is dependent on the spacing between the anchor plate and the outer edge of the concrete floor. As u_1 is larger than u_0 the stress levels for u_1 are significantly lower but the general shapes of the plots remain the same. The plots show for each anchor point 1-50 their stress levels for each layout of that case and load combination (dots). The line is shown to clarify the general level of stress and to more easily compare results.

7.1 Regular floor

First the results for the regular floor will be shown. Below plots can be found of the load combination LowWaterSummer at u_0 and u_1:
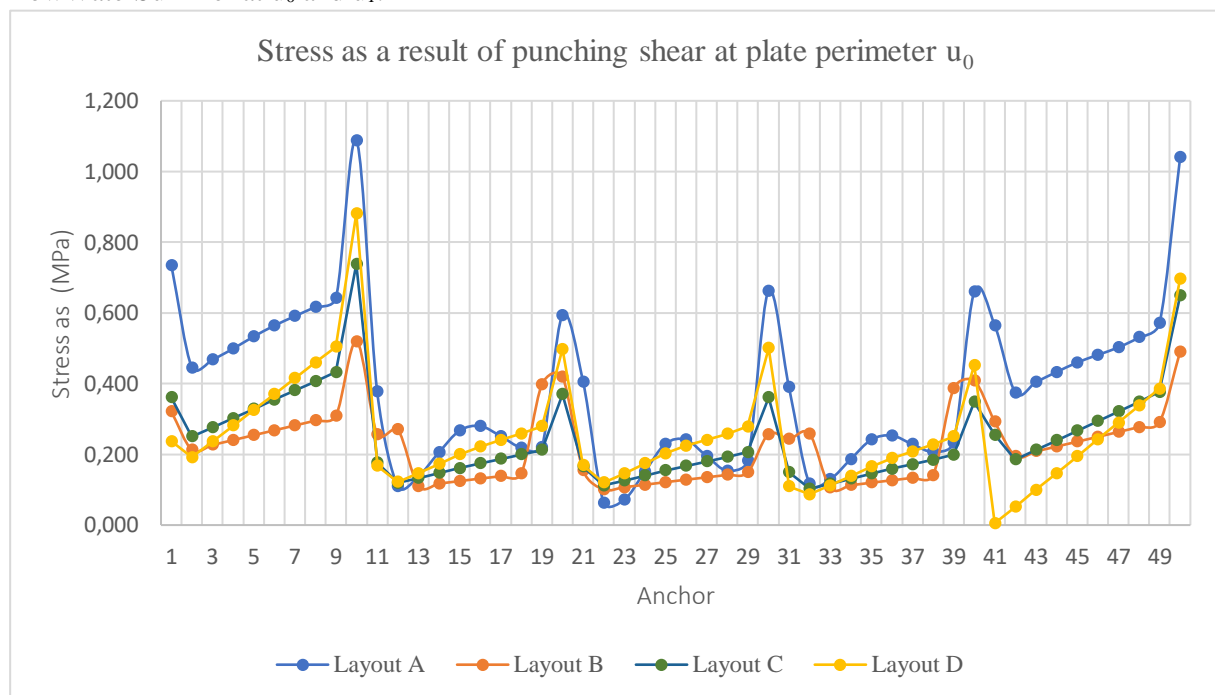
Figure 22: Stress Diagram regular floor LowWaterSummer perimeter u0

Layout A shows in the graph the highest overall stress with an exception for a few anchor points. These exceptions are particularly noticeable for the stress results for layout B at anchor points 12, 19, 32 and 39. This is due to the fact that the perimeter u_1 of Layout B is by far the largest, combined with the location of these particular anchor points their identity switches from an internal column (which is still the case for layout A, C and D) to a corner column (see Figure 50 and Figure 51 in 12.3.1). This results in a u_0 perimeter of only two sides of the plate rather than the full four sides, halving its perimeter from 1.4 m to 0.7 m. Additionally as stated in chapter 4.5.1 the β-value for corner columns is 1.5 compared to 1.15 for internal columns. For these two reasons the stress levels spike up at these locations with more than a magnitude of 2.6 compared to a relative internal column. Further the layouts B-D are more linear at internal anchor points (12-19, 22-29, 32-39) compared to more fluctuating graph of layout A. This is a direct result of more fluctuating forces VEd per anchor in layout A.
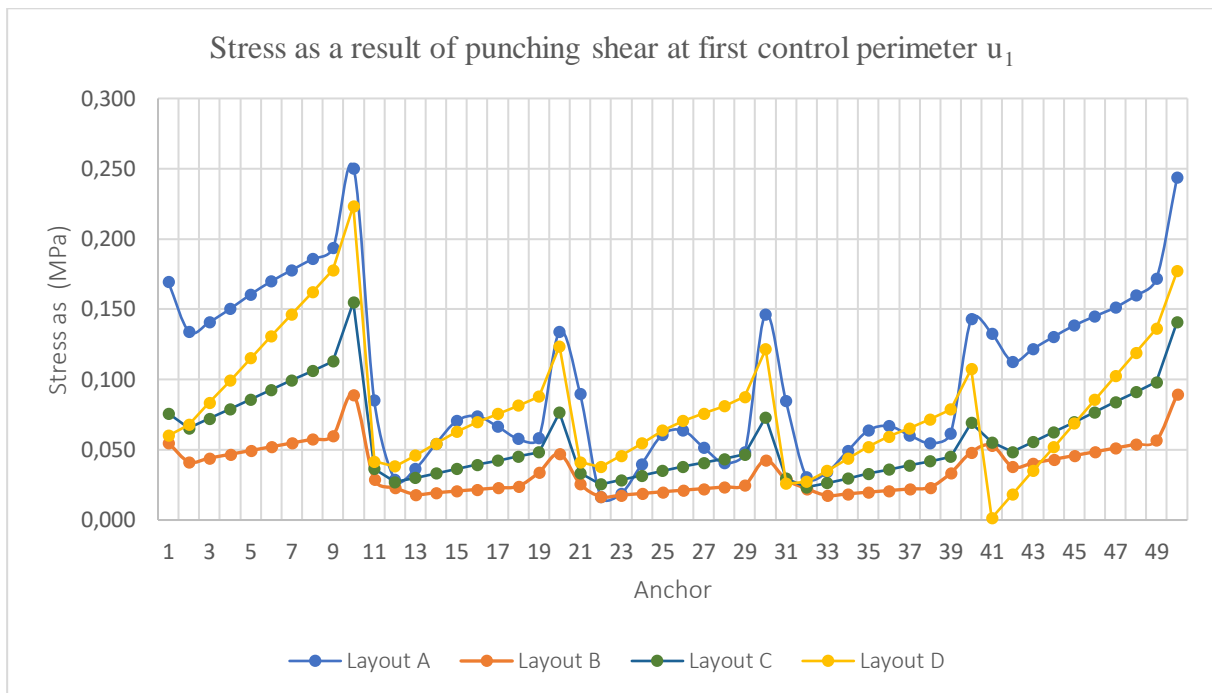
Figure 23: Stress Diagram regular floor LowWaterSummer perimeter u1

The second graph (Figure 23) showing the stress levels of the punching shear for load combination LowWaterSummer at the first control perimeter u_1. This plot displays a quite similar shape to the results at u_0. The main difference is the overall stress level being significantly lower with a maximum of around 0.25 MPa to a maximum of 1.1 MPa at u_0. Further the exceptions for anchor points 12, 19, 32, 39 for layout B are much less prominent as now control perimeter u_1 is taken into the equation which does not diverge much from the internal control perimeter (8.230 m vs 8.457 m).

HighWaterWinter

Below the graphs are plotted for the stress levels exerted during the HighWaterWinter load combination. In contrary to the LowWaterSummer load case this load case showed both compressive and tensile net forces (at different anchor point locations) for multiple layouts (Figure 59 appendix 12.3.2).
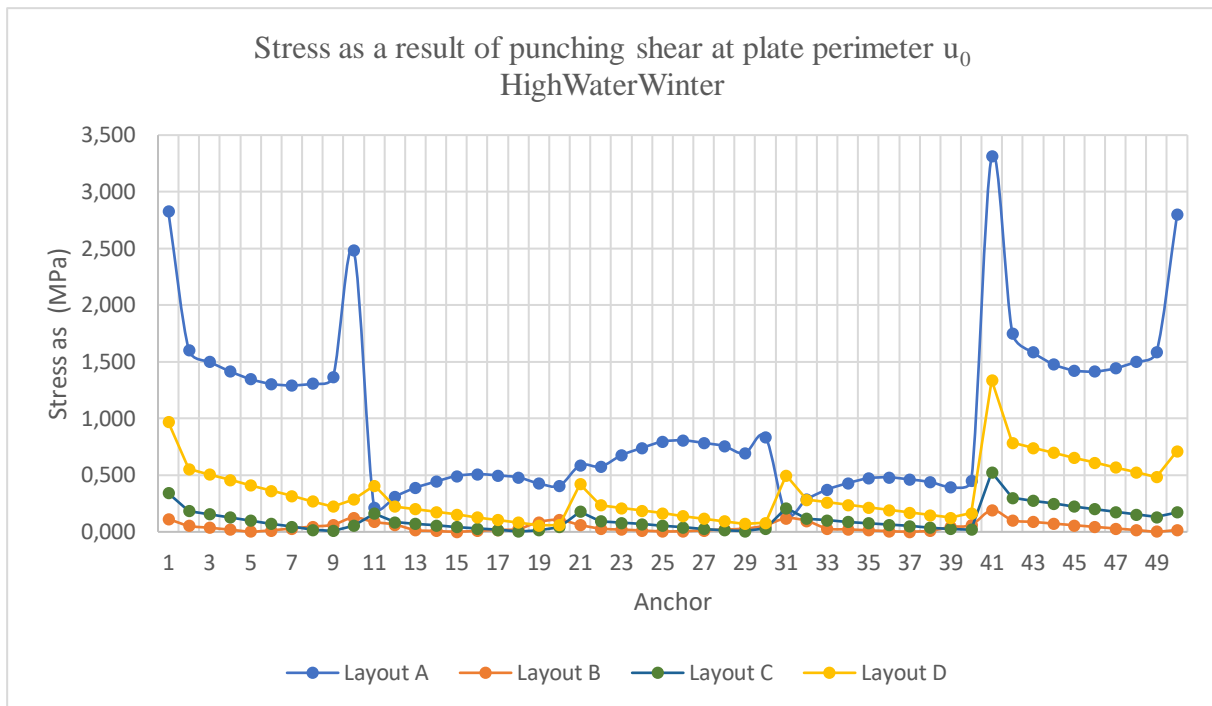
Figure 24: Stress Diagram regular floor HighWaterWinter perimeter u0
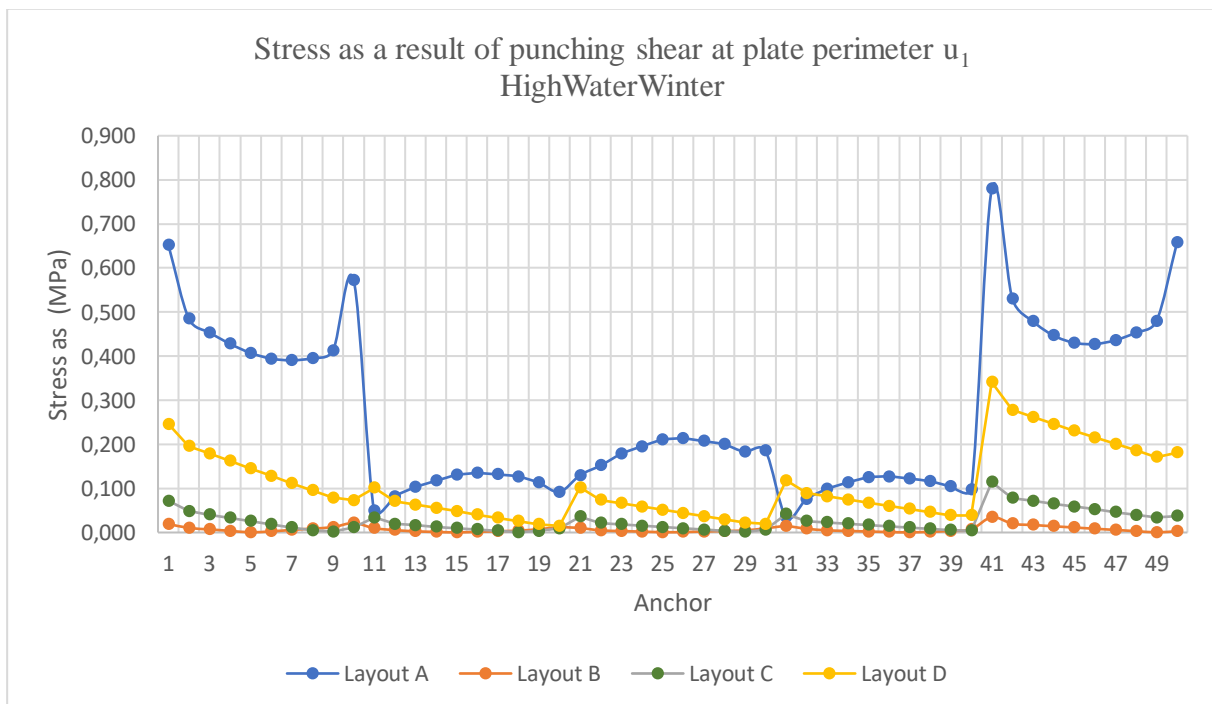
Figure 25: Stress Diagram regular floor HighWaterWinter perimeter u1

The result for both graphs are rather similar showing that layout A experiences far greater stress with an exception for anchor points 11, 31 and 32 of layout D.

UNIVERSITY
OF TWENTE.

anteagroup

7.2 Underwater concrete floor

Now the results for the underwater concrete floors will be considered, the results are shown for the initial placement of the underwater concrete floor and a final situation including loads that are not present during the initial placement. Again first the results for the LowWaterSummer load combination is addressed.

LowWaterSummer

    Initial placement
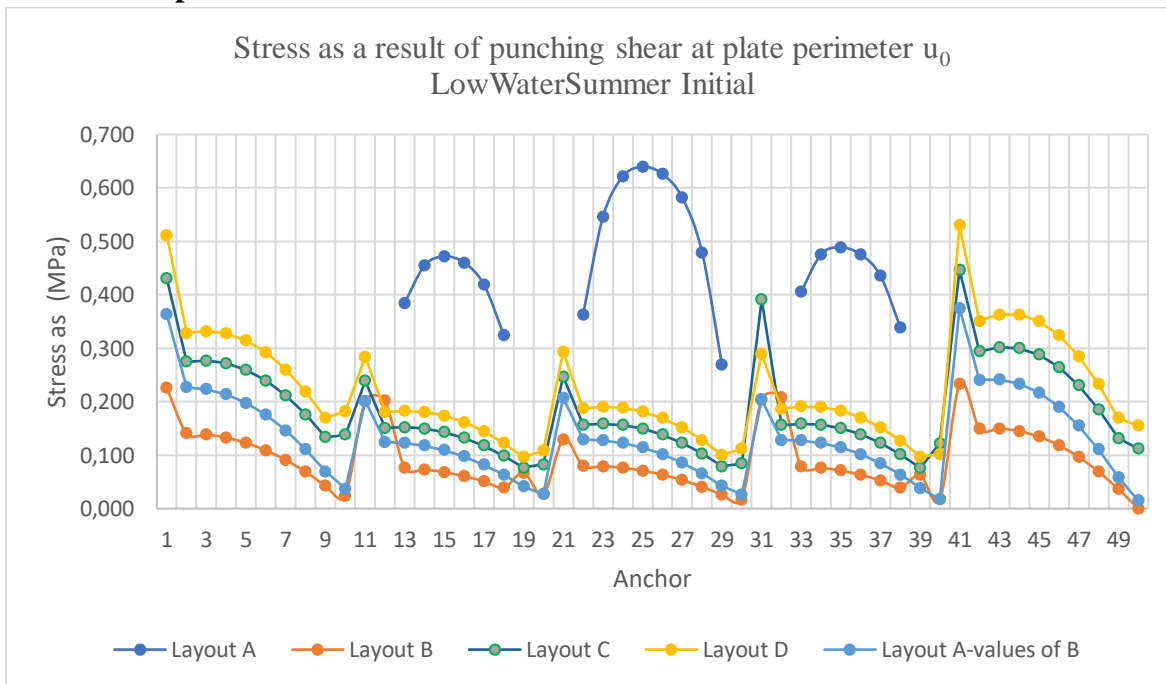
Figure 26: Stress Diagram UWC floor LowWaterSummer perimeter u0 initial
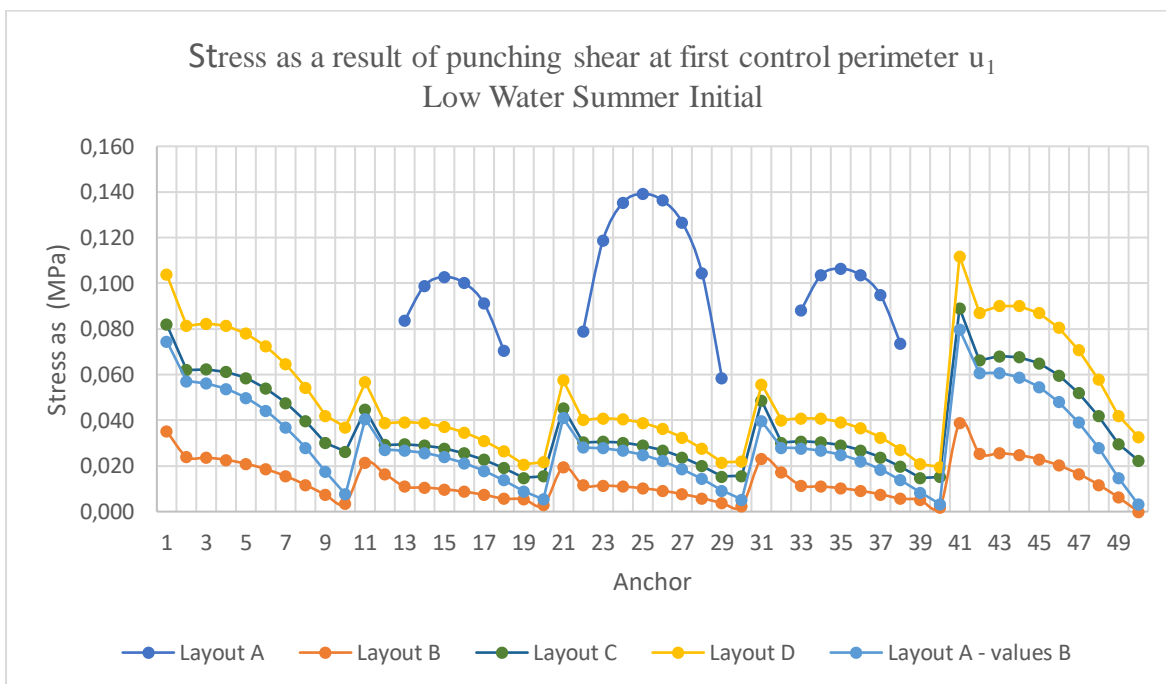
Figure 27: Stress Diagram UWC floor LowWaterSummer perimeter u1 initial

As can be seen in the graphs of Figure 26 and Figure 27 the results for layout A are excessively scattered compared to the other layouts, with very high peaks and low throughs. And a bumpy section for the internal columns. In contrary to the quite stable layouts of B,C and D, with occasional peaks for corner columns. Therefore a line has also been plotted for layout A using the net forces VEd of layout B as both layouts have an equal floor thickness. This gives a following the overall shape of the other layouts approximately at the height of layout C.

Final situation
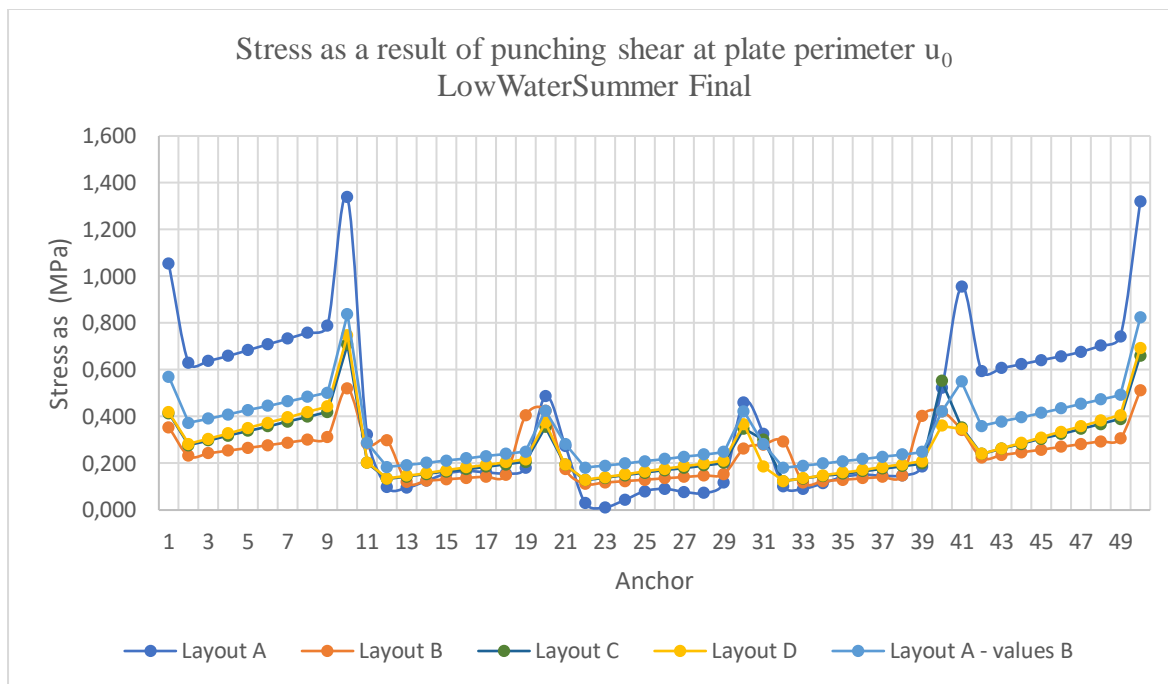
Figure 28: Stress Diagram UWC floor LowWaterSummer perimeter u0 final
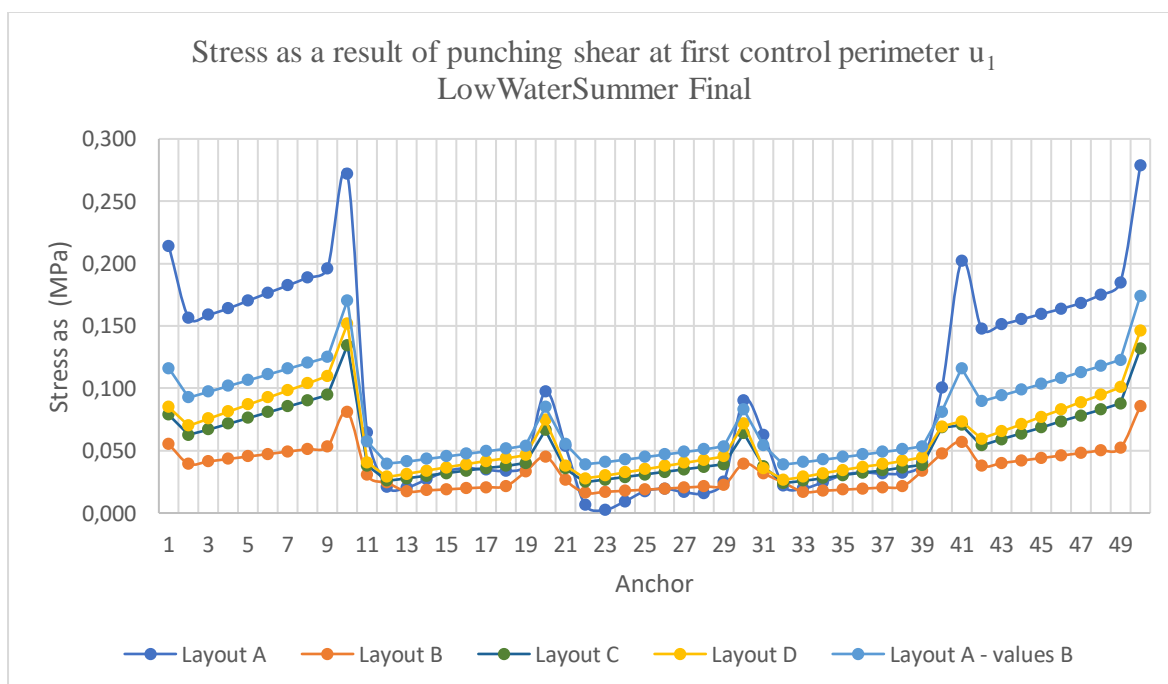
Figure 29: Stress Diagram UWC floor LowWaterSummer perimeter u1 final

UNIVERSITY OF TWENTE.

anteagroup

The diagram in Figure 28 and Figure 29 show de results for the final situation of the underwater concrete floor. The shapes of these graphs are much more similar to each other than during the initial placement. Despite, here it is chosen to also include layout A with net forces of B as it was done for the initial placement. The stress of layout A is easily the highest at corner and edge columns (1-10, 41-50). But does go significantly down for the internal columns and at some locations shows even the lowest stress levels. This is another reason why the layout A with net forces B was chosen to include. These results follow the same trajectory to the other layouts but at higher stress levels.

HighWaterWinter

Initial placement

The results for the floors at a the HighWaterWinter load combination during the initial phase are shown in the following diagrams.
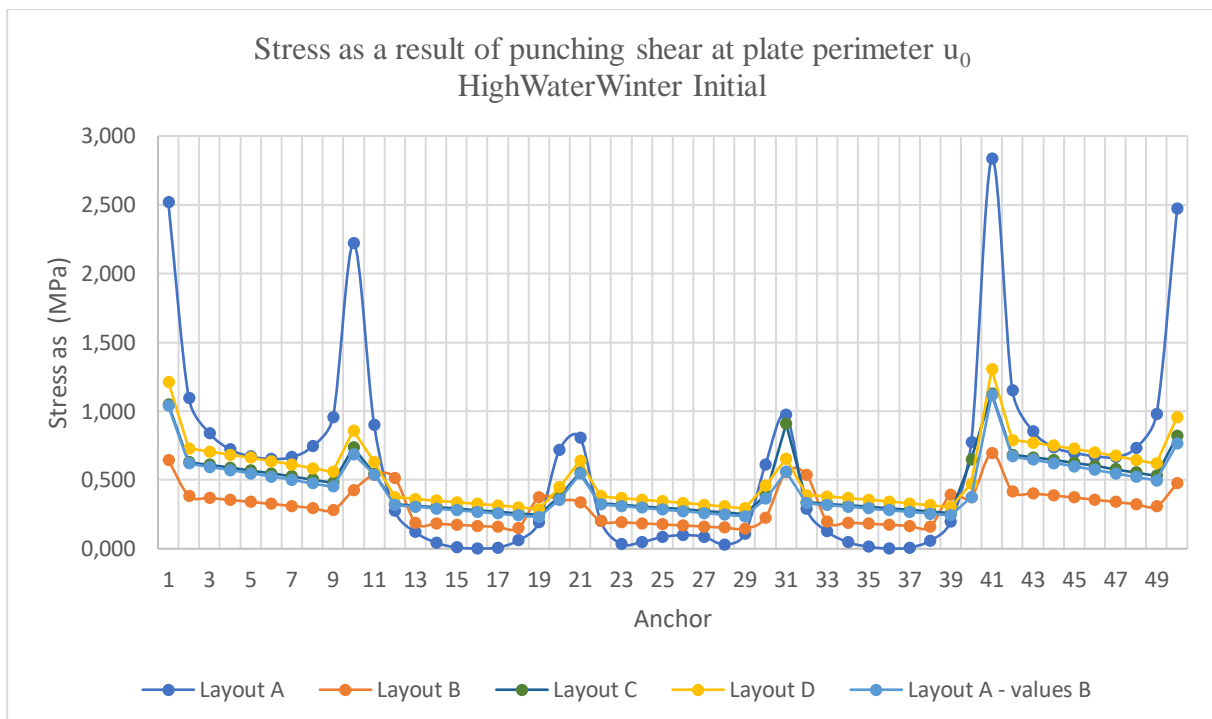
Figure 30: Stress Diagram UWC floor HighWaterWinter perimeter u0 initial
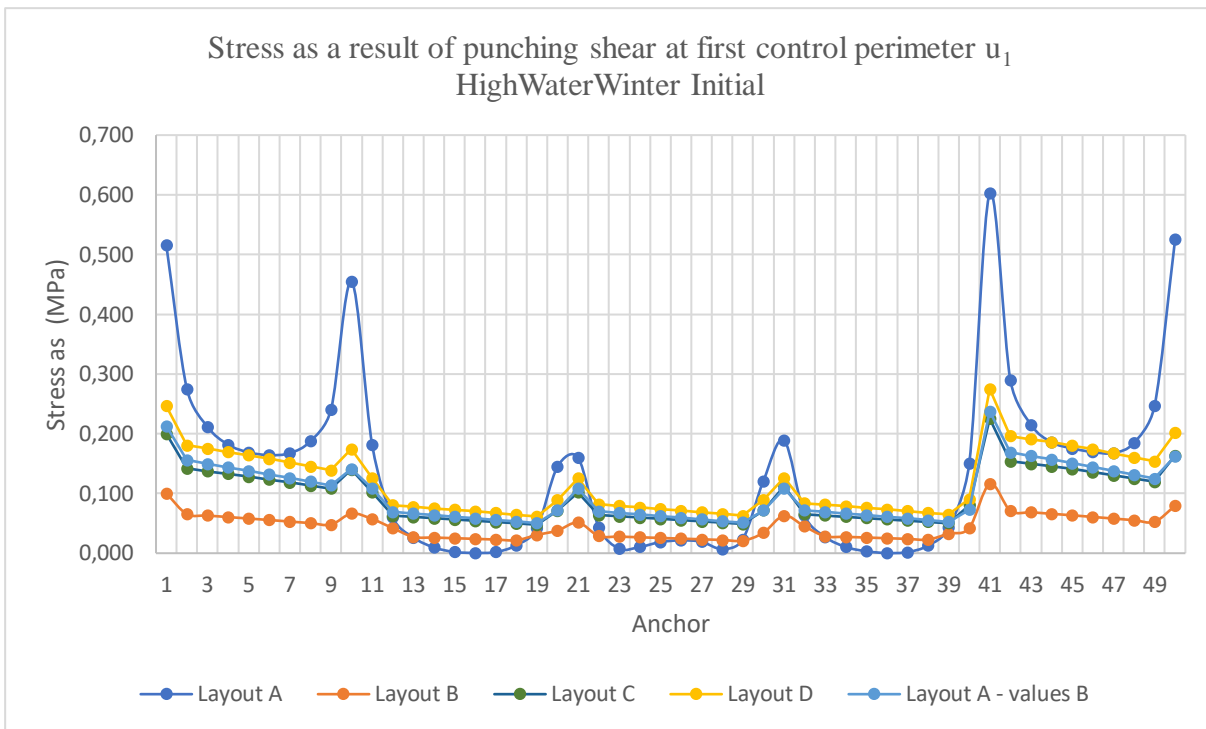
Figure 31: Stress Diagram UWC floor HighWaterWinter perimeter u1 initial

The diagrams show very high peaks and very low throughs at the corners and internal columns respectively for layout A. While the other layouts with double anchors keep a stable shape similar to the other cases. For this reason again an additional graph is included using layout A with net forces of B. This results in an outcome of an almost identical path with layout C.

Final situation
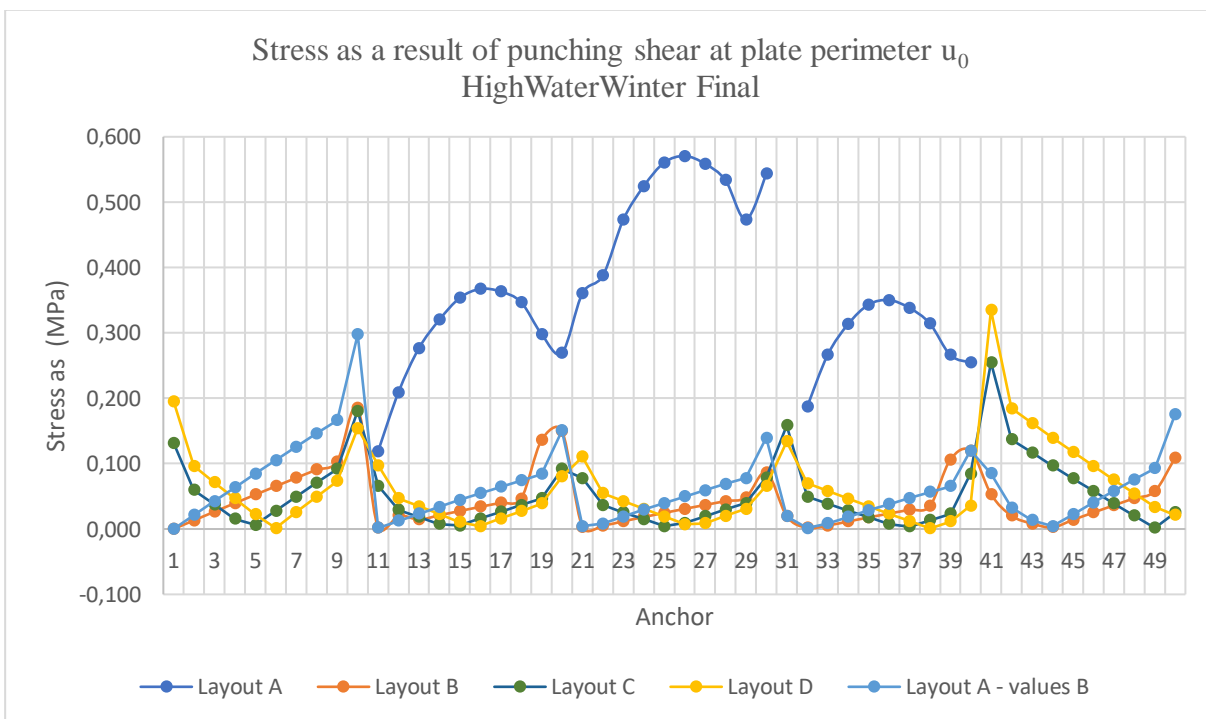
Figure 32: Stress Diagram UWC floor HighWaterWinter perimeter u0 final

UNIVERSITY OF TWENTE.

anteagroup
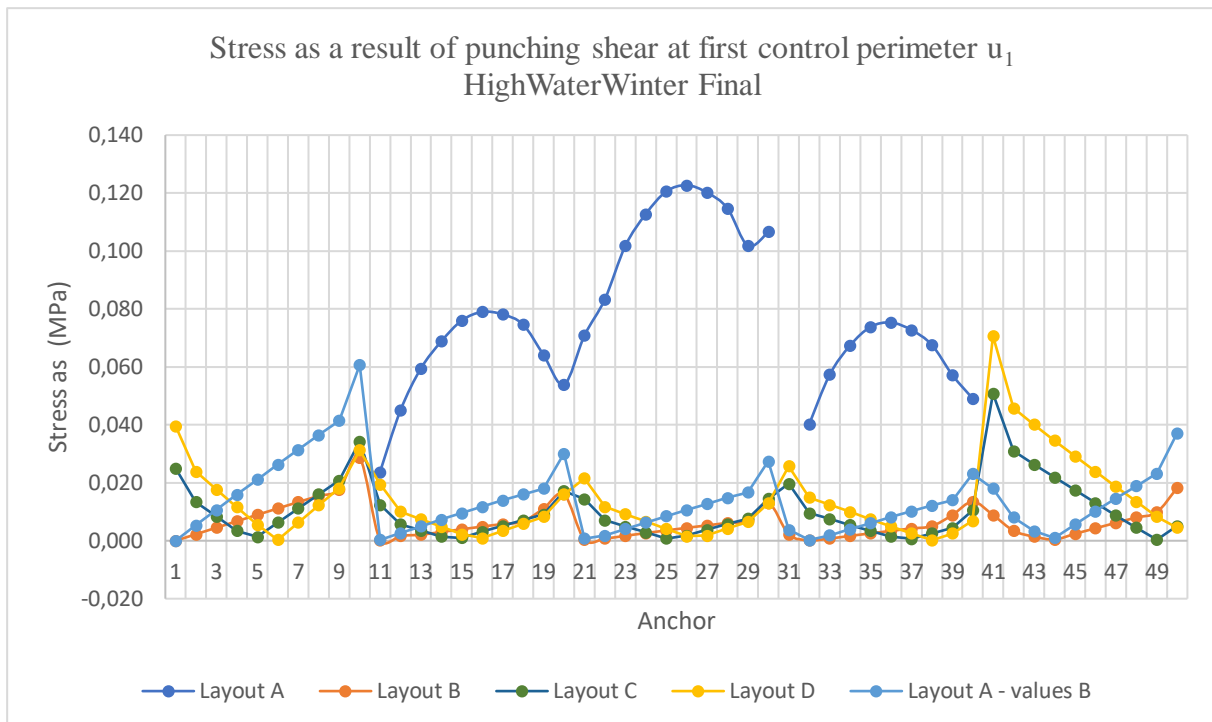
Figure 33: Stress Diagram UWC floor HighWaterWinter perimeter u1 final

In the final situation all layouts including the additional layout is close to zero except for layout A.

Due to high peak values of Layout A in many diagrams of the UWC floor, additional diagrams have been provided in appendix 12.3.3 which show some of the diagrams without the extreme peaks of Layout A. This makes it easier to see and compare the results of the other layouts which are now hard to distinguish.

8 Discussion

The objective of this research was to find and form numerical data to support the idea of a double anchored pile to be more beneficial compared to the ordinary single anchored pile. As a consequence of the idea that a double anchor could reduce a floor's thickness this research topic arose.

As contemplated the results showed a favour towards the double anchored floors. Even despite the rough shape of the results of Layout A, which seemed to be exceptionally odd at some instances. By introducing a fifth data set/ layout which uses the layout of A but the input data of B the overall shape of the graph was adjusted to be more fitting with the double anchored layouts. This made it possible to draw positive results even when excluding the results of the original Layout A.

The stress levels on the concrete over the first control perimeter are heavily reliant on the effective height. The formula for the first control perimeter u_1 is $u_1 = u_0 + 4\,\pi * d_{eff}$ this shows how much the effective height affects the control perimeter. The main idea with implementing a double anchor is to drastically increase this effective height by placing the anchor further away from the edge. To execute this method it is crucial to use two anchors as placing the anchor far away from one edge directly means placing it closer to the other.

What was surprising to see at first was the results of Layout D with an effective height equal to that of Layout A still outperforms Layout A. Showing that increased effective height is not directly necessary to lower the stress levels. This is due to the fact that by decreasing the floor's thickness the load of the selfweight drastically changes. Therefore the net force on the anchors change and thus the stress reduces even at equal effective heights. This, however, only applies for the final situation. Figure 62 and Figure 63 show that during the final situation the net force is mostly compressive (blue) therefore a decrease in selfweight of the floor (compressive load) is beneficial for reducing the net force. While in the initial placement the net force shows to be more tensile (Figure 60 and Figure 61), hence removing compressive load here is not beneficial and actually increases the net force. This correlates well with the results as layout D has higher stress values than Layout A – values B during initial placement. But scores better during the final situation and even scores not far off of Layout C's results. The disadvantage during the initial placement could on the other hand be easily adjusted in the real world with temporary removable weights.

Layout C showed very stable results similar to shape of Layout B only at higher stress values. Layout C did perform very close to Layout A (– values B). Where in some of the situations it outperformed Layout A (– valuesB), but in others it lost marginally to this layout. Which was mostly dependent on the overall tensile or compressive net force, here the same phenomenon of decreased compressive load applies as for Layout D with its associated effect. Overall the results for Layout C and A-valuesB were very similar. For the UWC layout C has a thickness of 800 mm compared to the 1000 mm of Layout A. Therefore Layout C takes the cake in an overall comparative analysis between all layouts. While Layout B easily showed the best results regarding low stress levels it does not reach the goal of saving materials which is a great objective and purpose to apply a double anchor originally. This is a trait that Layout C does achieve well with a reduction of 20 percent in the (underwater) concrete floor. All whilst managing to keep up similar performance as Layout A. Layout D could be the winner if additional temporary weights were to be installed during the initial placement. This would lead to a floor reduction of 25%.

9 Conclusion

In conclusion the main question to be answered in this research is: ***"What is the effect of a double anchor plate on GEWI-piles on force distribution/punch capacity in an underwater concrete foundation compared to that of a single anchor plate?"*** . Another question to further elaborate on this effect: ***"How beneficial is a double anchor plate on GEWI-piles?".***

The diagrams in the results show promising outcomes. The stress levels for layout A, the control floor, score overall higher as expected. Layout B which has equal thickness as Layout A but two more favourably placed anchors in contrary to one shows significantly better/lower stress levels. Layout C and D also equipped with double anchors but lesser floor thicknesses follow a similar path as Layout B but at slightly higher stress levels reaching closer towards the results of Layout A.

Layout B showed the best results, namely the lowest stress levels, despite it does not decrease the floor thickness which was one of the core purposes to investigate this matter to save on material use. Layout C and D do decrease floor thickness with 25% and 37.5% respectively for the regular floor and 20% and 25% respectively for the underwater concrete floor. While choosing the thinnest floor would result in the most material savings, layout D surpasses the stress levels of Layout A regularly in the diagram of Figure 23. Therefore for the regular floor layout C is preferred as it scores consistently lower stress levels while saving 25% in floor thickness. For the underwater concrete floor the same approach is applied. While Layout A is often much higher (regarding the peaks) the adapted graph of layout A (using netforce of Layout B) is closer to Layout C. In most occasions layout D experiences higher stress levels than the adapted Layout A. For some occasions Layout C also excess the stress levels of the adapted Layout A, in these instances the increase is quite minimal. In other occasions the results are almost identical, and in others Layout C achieves lower stress levels. For this reason also for the underwater concrete floor Layout C is preferred, and a reduction of 20% in floor thickness can be realized.

To finalize and answer back on the main research questions, repeated at the start of this chapter. The simple answer to this question is that when GEWI-piles are equipped with double anchor plates the anchorage results in more punch capacity/ lower stress as a result of punching compared to the use of a single anchor. Realistically a reduction of 20% in floor thickness can be realized without it being at the expense of the punch capacity/stability.

10 Limitations and future research

Complications/limitations and uncertainties

Constructing the model in SCIA Engineer was not smooth sailing as multiple complications came forward, which caused in deviations or uncertainties. First, the decision was made to not include the curvature of the segment as it is designed to be in the real world. The model made by Antea Group to perform calculations for the official project also did not include this curvature. Therefore it seemed fit to exclude the curve in this model as well. As SCIA does not allow curves in plates or wall including the curvature would mean a great amount of angles.

Secondly, SCIA was not able to calculate punching shear on slanted floors. While the tunnel segment has an incline of about 3.8°, this could not be realized in the model. The structure had to be adapted/flattened to make the floor level. This resulted in equal wall height on both the north and south side of the structure and altered the water and ground pressure load slightly.

Another obstacle that was encountered was the impossibility to insert two anchors in a single plate (floor). To work around this issue two floors with a heartline at different elevations were placed overlapping into each other. The floors were connected to each other by the walls or rigid connections in cases where the walls were not placed. This double floor did result in double selfweight of the floor, thus increasing the total net compressive load. To bypass this emerged problem a custom material composition was made which held identical properties as the regular C30/37 concrete composition but at half the weight. Each layout utilizing this double floor was equipped with this custom concrete composition.

Further, despite punching the anchors at the heartline of a plate, SCIA registered the effective height (d_{eff}) as if the punching object was connected below/above the floor rather than at the heartline. Therefore taking the entire thickness of the plate minus tolerances to determine the effective height instead of the distance between the heartline and the edge minus tolerances. This resulted in much higher effective heights. Consequently, significantly increasing the perimeters and decreasing the stress/perimeter. It was not possible to manually adapt the effective height, however it was possible to change a factor in the settings that was used to define the first control perimeter u_1. The customary equation that is used to define the distance to the first control perimeter is $2d_{eff}$. For each layout the new factor (former 2) was determined to correct for the mistaken effective height. For example, in Layout A with a floor thickness of 800 mm and a heartline at 400 mm, where SCIA takes d = 0.71m but it should have been d = 0.31m. The new factor would result to 0.87 as $0.87*0.71 \approx 2*0.31$. This made it possible for SCIA to automatically calculate the correct perimeters meant for a connection somewhere within the floor instead of right below/above the floor.

A fifth imperfection/deviation compared to the used model by Antea Group is the difference in traffic loads. Antea Group used a total of 82 different variations of traffic loads of which 1 was a surface load spanning the entire surface, the other 81 were partial surface loads. The model used for this research only used the 1 surface load and 1 variation of the 81 partial loads. The total load of the partial loads were identical for each variation, only the location/order of the loads varied.

Finally, an odd emergence was the different net force behaviour of Layout A (the control floor) which used only a single floor with a single layer of anchors. While the other layouts used double floors/double anchor layers one layer strictly absorbing compressive forces and the other strictly absorbing tensile forces. Layout B,C,D resulted in proportionate gradual distribution of net force for each different case and load combination. Layout A on the other hand had very divergent results

regarding net force, with sudden peaks or throughs or very high compression at the corners and edges together with high tension at internal anchors and vice versa. Figure 58 to Figure 63 in appendix 12.3.2 show the irregularities of the net force distribution at Layout A. Also the proportionate gradual distribution at layout B-D are visible in the figures. The reason for this occurrence has not been found nor could be fixed. For this reason for very divergent net forces at Layout A, some cases included adapted results for Layout A that used net force values of Layout B as input values.

Future research

In future research it would be interesting to look at environmental/sustainable side of the reduction. As for the results of this research paper a quantification of the possible reduction in floor thickness is determined. To ultimately alter the regulations it would be helpful to see what and how exactly the reduction of floor thickness translates to savings in price and effects to sustainability aspects, such as; emission of harmful substances (CO_2), and lifecycle of the underwater concrete floors. The reduction of floor thickness and therefore reduction of concrete use is apparent, on the other hand it does increase the use of metal in the floors by additional anchor disks. It therefore it cannot be confidently said that a double anchor is beneficial in terms of sustainability without further investigation.

Moreover, this research is entirely based on the results simulated and calculated by SCIA Engineer. While SCIA is a very trustworthy and respected software, simulations do not always correlate to real world phenomenon. Especially in new fields like such where a bypass was needed to be able to model the double anchored floor in the first place and a lot of limitations are attendant. As long as a double anchored floor is not yet fully integrated in the software by professionals the results can diverge from true consequences. For this reason it would be intriguing to see a similar research being carried out with real concrete floors and GEWI-anchors in labs. This will provide real world results and possibly show additional consequences/drawbacks not showed in simulation. Real lab research would be a very convincing addition to show the benefits of double anchored piles in underwater concrete floors. And could be an inciter to include such flooring methods in engineering software like SCIA.

11 Bibliography

Alessandro Flora, R. L. (2018). Foundations. In B. R. Peter T. Bobrowsky, *Encyclopedia of Engineering Geology* (pp. 369-371). Napoli: Springer Cham.

Arno Poels, J. R. (2022, november 23). Ontwerp Singelgrachtgarage-Marnix. *CEMENT 7*, pp. 18 - 28.

Das, B. M. (2011). *Principles of Foundation Engineering, SI.* Stamford: Cengage Learning.

Doohyun Kyung, D. K. (2017). Vertical load-carrying behavior and design models for micropiles considering foundation configuration conditions. In *Canadian Geotechnical Journal* (p. 234+). NRC Research Press.

DYWIDAG. (2021). *Geotechnical Systems.* Unterschleissheim: DIBt.

DYWIDAG. (2024, April 2). *GEWI® piles support Bowon Office Building in Seoul*. Retrieved from dywidag-formties: https://www.dywidag-formties.com/projects/1997-info-6/gewi-piles-support-bowon-office-building-in-seoul/

DYWIDAG. (2024, April 2). *GEWI® Piles used for Important Train Connection from Munich to Verona*. Retrieved from dywidag-formties: https://www.dywidag-formties.com/projects/2011-info-19/gewi-piles-used-for-important-train-connection-from-munich-to-verona/

Dywidag-formties. (2024, 3 12). *GEWI® piles support Bowon Office Building in Seoul*. Retrieved from Dywidag-formties: https://www.dywidag-formties.com/projects/1997-info-6/gewi-piles-support-bowon-office-building-in-seoul/

DYWIDAG-Systems International GmbH. (2021). *DYWIDAG Geotechnical Product Range.* Koenigsbrunn.

H.G. Kempfert, F. B. (2013). *Raft foundation on floating micropiles in soft soils.* Kassel: Institute of Geotechnics and Geohydraulics .

Hans-Georg Kempfert, B. G. (2006). Micropiles. In B. G. Hans-Georg Kempfert, *Excavations and Foundations in Soft Soils* (pp. 349-352, 378-382). Kassel: Springer.

NEN. (2011, november 1). *Eurocode 2: Ontwerp en berekening van betonconstructies - Deel 1-1: Algemene regels en regels voor gebouwen.* Retrieved from nen: https://connect.nen.nl/Standard/Detail/159356?compId=10635&collectionId=0

NEN. (2015, june 1). *Uitvoering van bijzonder geotechnisch werk - Micropalen.* Retrieved from nen: https://connect.nen.nl/standard/Detail/207366?compId=10635&collectionId=0

NEN. (2017, november 1). *Geotechnisch ontwerp van constructies - Deel 1: Algemene regels.* Retrieved from nen: https://connect.nen.nl/Standard/Detail/3535337?compId=10635&collectionId=0

Paul J. Sabatini, B. T. (2005). *Micropile Design and Construction (Reference Manual for NHI Course 132078) .* Dallas.

SBRCURnet. (2014). Dimensionering en toetsing van verbindingen. In *CUR-Aanbevelinv 77:2014 Rekenregels voor onbewapende onderwaterbetonvloeren* (pp. 43-45). Rotterdam: SBRCURnet.

Stephan van Tilburg, R. A. (2021, april 1). Grensverleggende parkeergarage. *CEMENT 7*, pp. 6 - 13.

12 Appendices

12.1 Segment 8 technical drawings

In Figure 34, Figure 35 and Figure 36 below the technical drawings of segment 8 of the bus underpass are displayed. The figures provide a side view, front view and top view respectively of the segment.
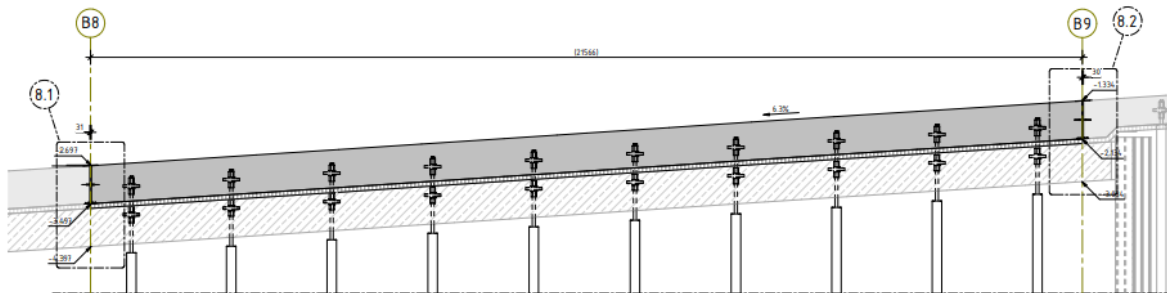
Figure 34: Technical drawing of the side view of segment 8
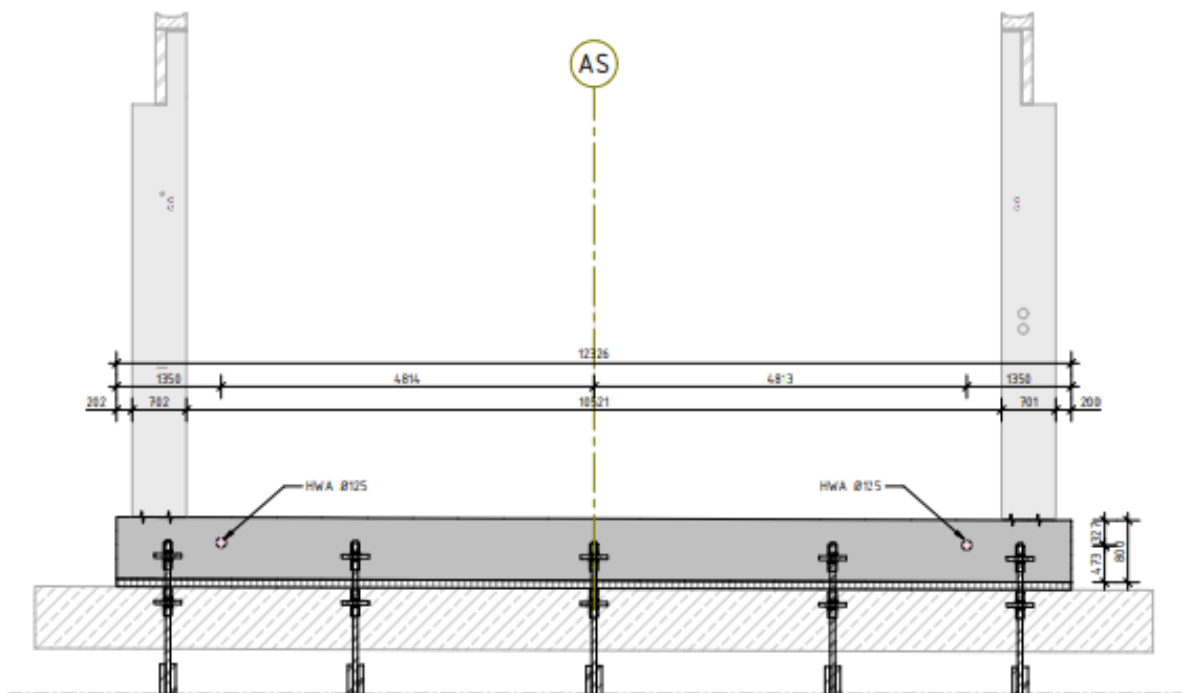
Figure 35: Technical drawing of the front view of segment 8 from the south side
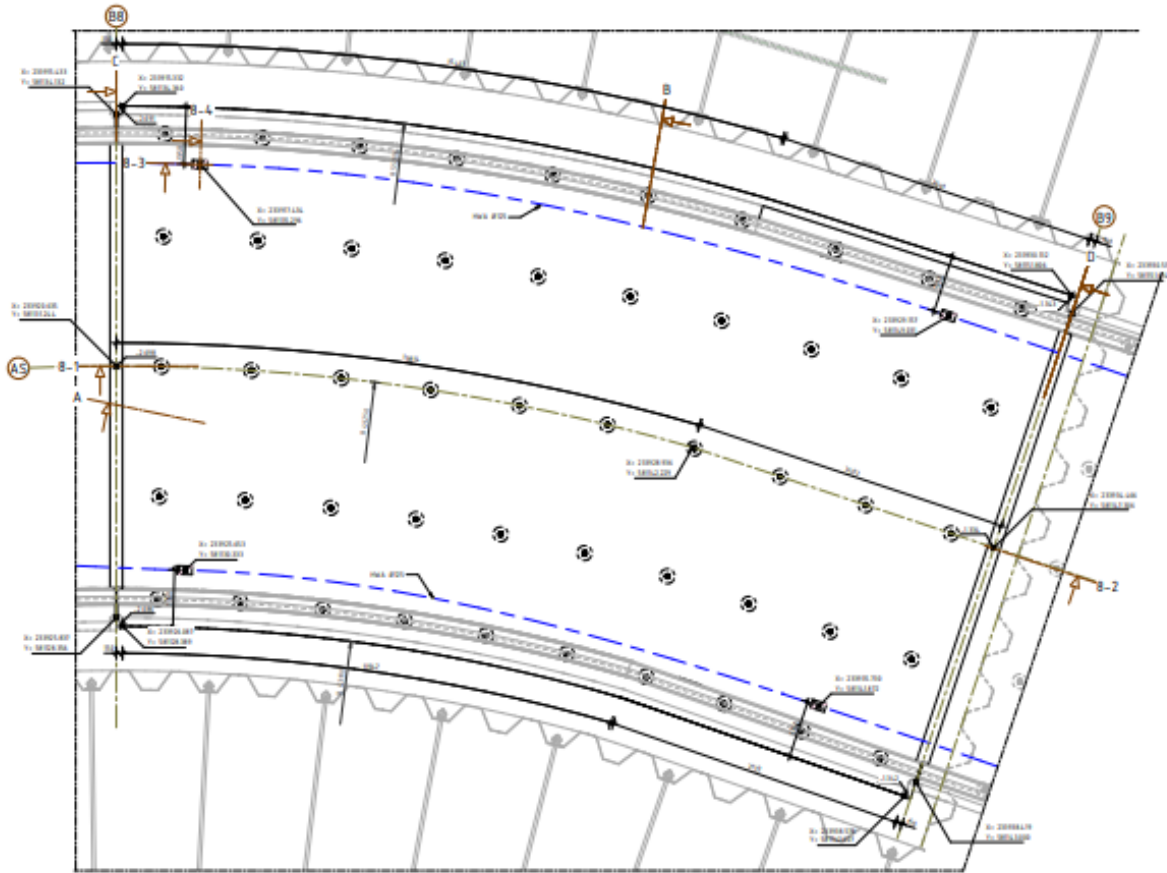
Figure 36: Technical drawing of the top view of segment 8

12.2 Loads

12.2.1   Resting

Figure 37 shows how the resting loads are placed in the model.
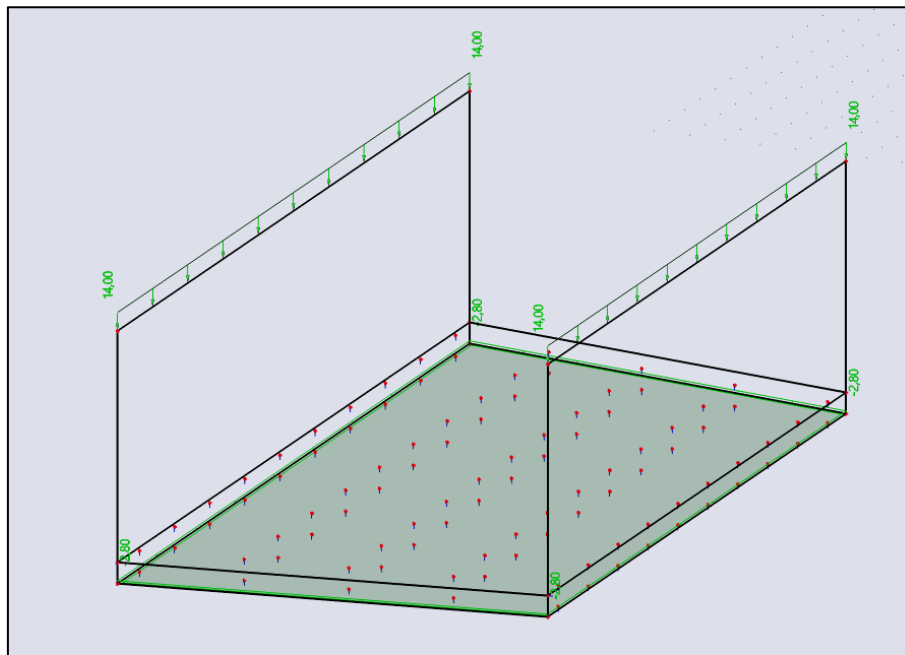
Figure 37: Resting load

12.2.2   Ground and water pressure

Ground and Water pressure North side

Figure 38 below shows the layout of elements of segment 8 and their elevation with respect to NAP +/- 0.000 m. Locations are numbered from 0-6 for which each later the vertical and horizontal loads will be determined.

Location 0: Top of the wall   (+ 3.400 m)
Location 1: Ground level   (+ 3.400 m)
Location 2: High water table   (+ 2.500 m)
Location 3: Low water table   (+ 0.500 m)
Location 4: Top of the floor   (- 1.330 m)
Location 5: Middle of the floor   (- 1.730 m)
Location 6: Bottom of the floor   (- 2.130 m)

UNIVERSITY OF TWENTE.

anteagroup
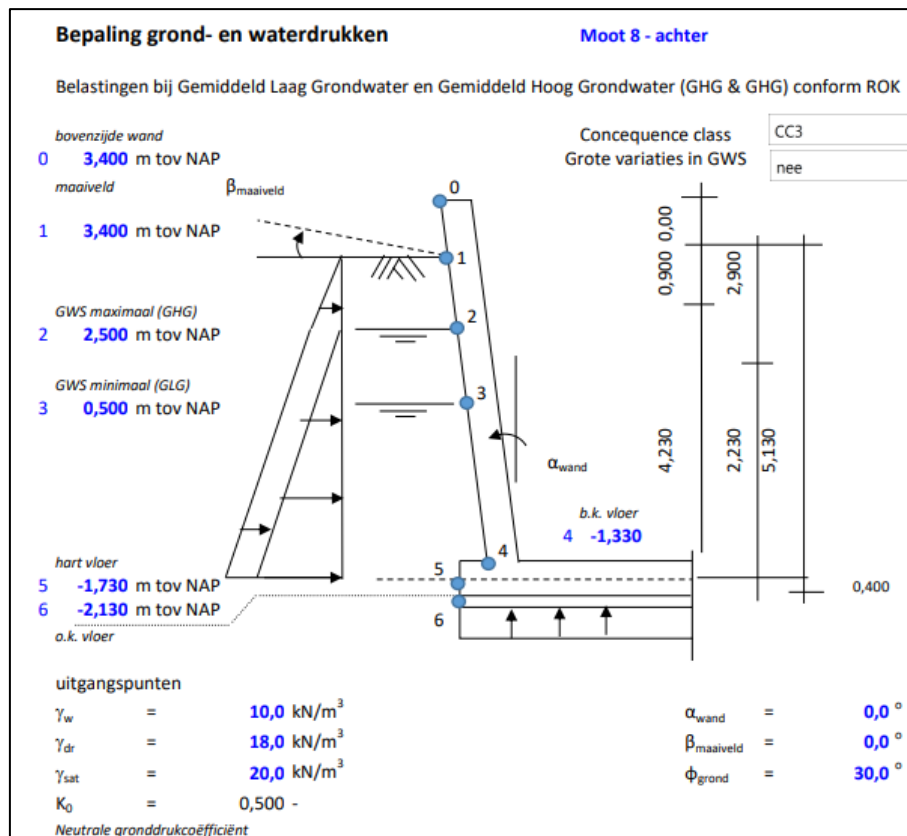
Figure 38: Overview ground and water pressure on segment north side

Table 4 and Table 5 below show the resulting loads of the ground and water pressure at a low and high water table respectively at the north boundary of the segment.

Table 4: Resulting loads north side low water table

North side low watertable (GLG)				
Location	Elevation w.r.t. NAP	Hor. water pressure	Vert. ground pressure	Hor. grain pressure	Combined hor. pressure
	[m]	[kN/m2]	[kN/m2]	[kN/m2]	[kN/m2]
0	3,400	0,0	0,0	0,0	0,0
1	3,400	0,0	0,0	0,0	0,0
2	2,500	0,0	16,2	8,1	8,1
3	0,500	0,0	52,2	26,1	26,1
4	-1,330	18,3	88,8	35,3	53,6
5	-1,730	22,3	96,8	37,3	59,6
6	-2,130	26,3	104,8	39,3	65,6

Table 5: Resulting loads north side high water table

	North side high watertable (GHG)				
Location	Elevation w.r.t. NAP	Hor. water pressure	Vert. ground pressure	Hor. grain pressure	Combined hor. pressure
	[m]	[kN/m2]	[kN/m2]	[kN/m2]	[kN/m2]
0	3,400	0,0	0,0	0,0	0,0
1	3,400	0,0	0,0	0,0	0,0
2	2,500	0,0	16,2	8,1	8,1
3	0,500	20,0	56,2	18,1	38,1
4	-1,330	38,0	92,8	27,3	65,3
5	-1,730	42,3	100,8	29,3	71,6
6	-2,130	46,3	108,8	31,3	77,6

Ground and Water pressure South side

Figure 39 showing the south side of the segment follows the same layout as Figure 38 with different elevations for locations 4-6.

Location 4: Top of the floor   (- 2.700 m)
Location 5: Middle of the floor   (- 3.100 m)
Location 6: Bottom of the floor   (- 3.500 m)
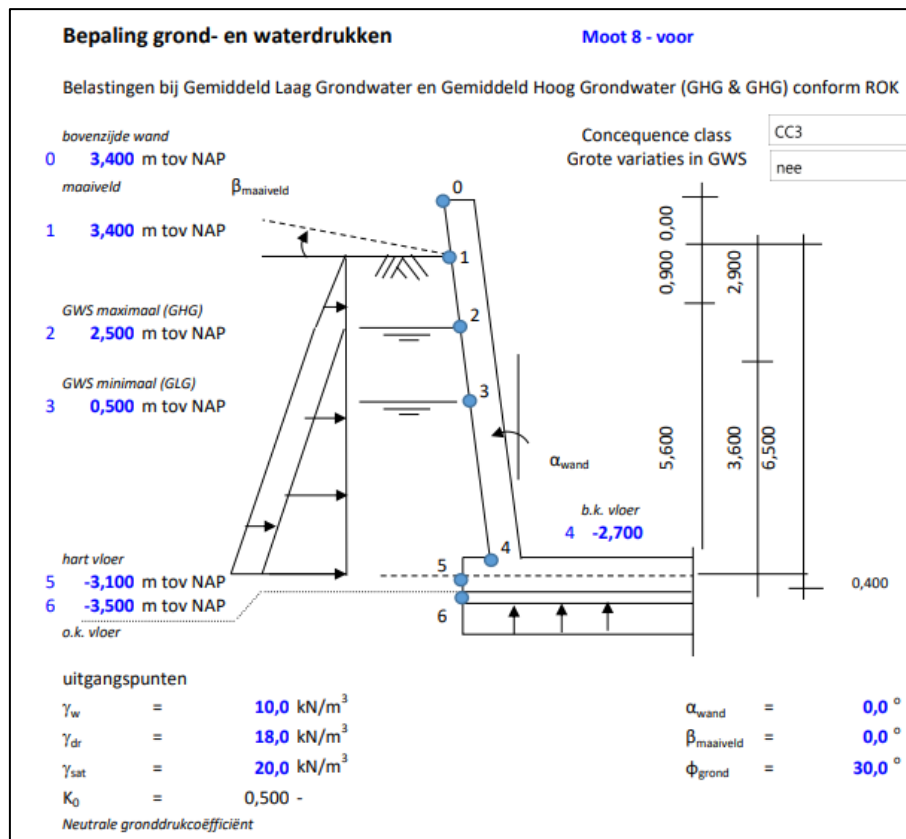
Figure 39: Overview ground and water pressure on segment south side

Table 6 and Table 7 below show the resulting loads of the ground and water pressure at a low and high water table respectively at the south boundary of the segment.

Table 6: resulting loads south side low water table

Location	Elevation w.r.t. NAP	Hor. water pressure	Vert. ground pressure	Hor. grain pressure	Combined hor. pressure
	South side low watertable (GLG)				
	[m]	[kN/m2]	[kN/m2]	[kN/m2]	[kN/m2]
0	3,400	0,0	0,0	0,0	0,0
1	3,400	0,0	0,0	0,0	0,0
2	2,500	0,0	16,2	8,1	8,1
3	0,500	0,0	52,2	26,1	26,1
4	-2,700	32,0	116,2	42,1	74,1
5	-3,100	36,0	124,2	44,1	80,1
6	-3,500	40,0	132,2	46,1	86,1

Table 7: Resulting loads south side high water table

Location	Elevation w.r.t. NAP	Hor. water pressure	Vert. ground pressure	Hor. grain pressure	Combined hor. pressure
	South side high watertable (GHG)				
	[m]	[kN/m2]	[kN/m2]	[kN/m2]	[kN/m2]
0	3,400	0,0	0,0	0,0	0,0
1	3,400	0,0	0,0	0,0	0,0
2	2,500	0,0	16,2	8,1	8,1
3	0,500	20,0	56,2	18,1	38,1
4	-2,700	52,0	120,2	34,1	86,1
5	-3,100	56,0	128,2	36,1	92,1
6	-3,500	60,0	136,2	38,1	98,1

Ground and Water pressure load

Figure 40 and Figure 41 show how the ground and water pressure loads are placed in the model for the low and high water table respectively.
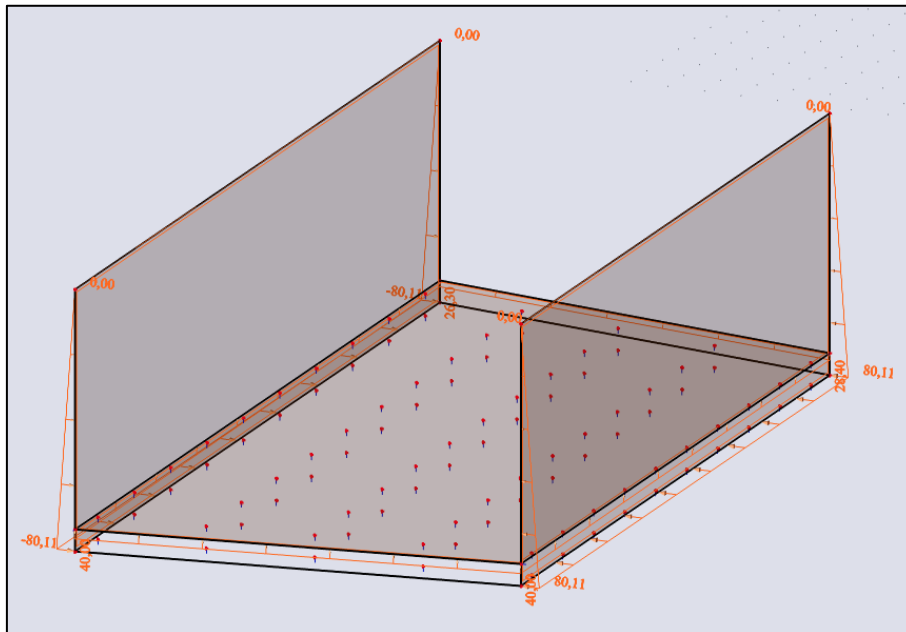
Figure 40: Ground and water pressure load low water table
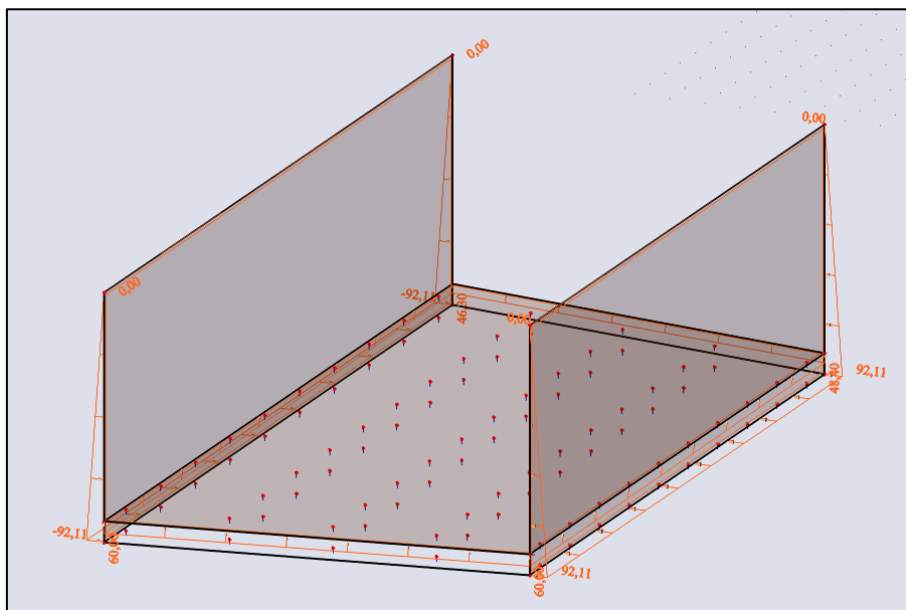
Figure 41: Ground and water pressure load high water table

12.2.3 Shrinking load

Figure 42 shows how the shrinking loads are placed in the model.
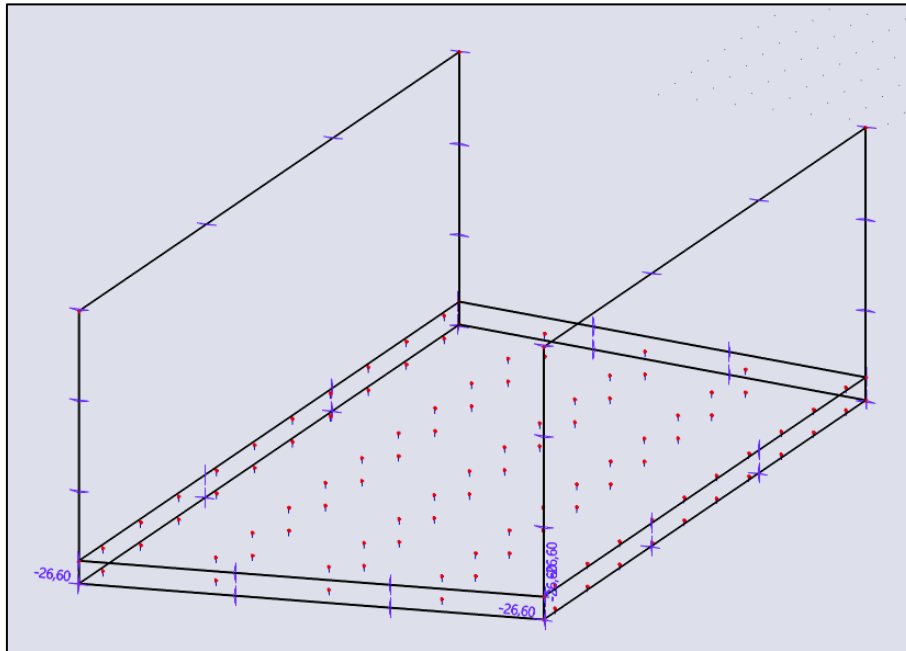
Figure 42: Shrinking load

12.2.4 Temperature loads

Figure 43 and Figure 44 show how the temperature loads are placed in the model for Summer and Winter temperatures respectively.
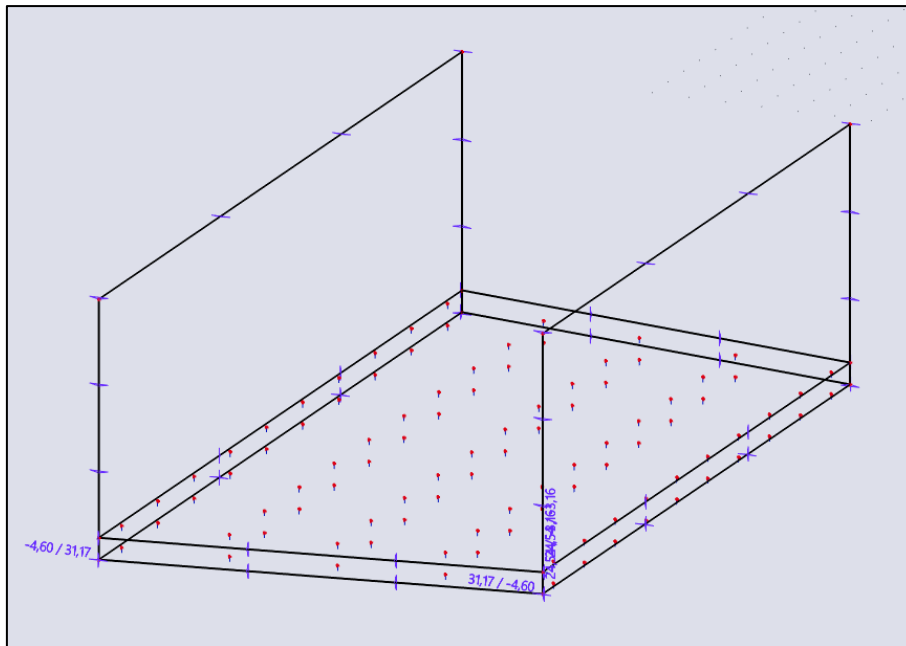
Figure 43: Temperature load Summer
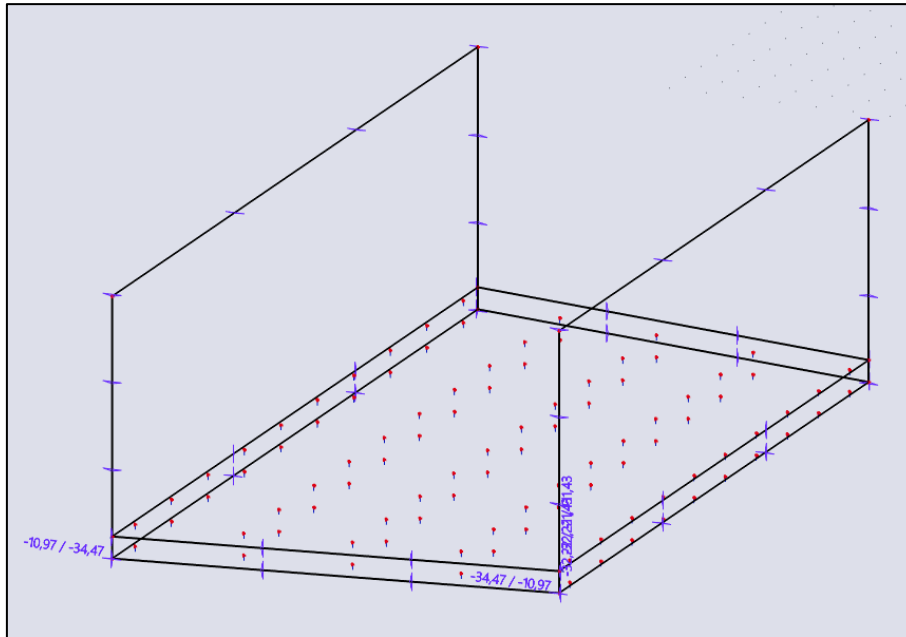
Figure 44; Temperature load Winter

12.2.5 Groundlevel load

Figure 45 shows how the Grounlevel loads are placed in the model.
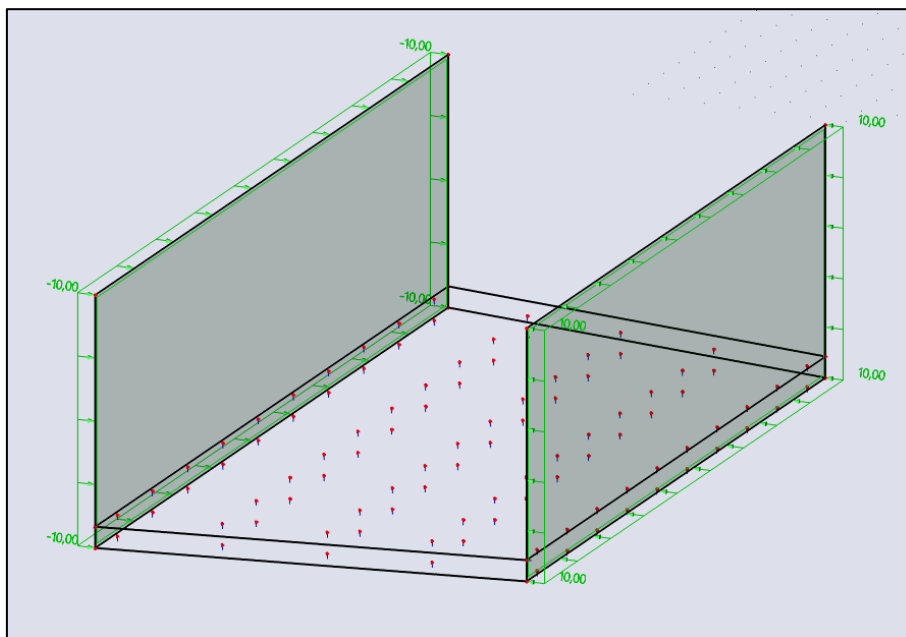
Figure 45: Groundlevel load

12.2.6   Clamping Load

Figure 46 shows how the clamping loads are placed in the model.
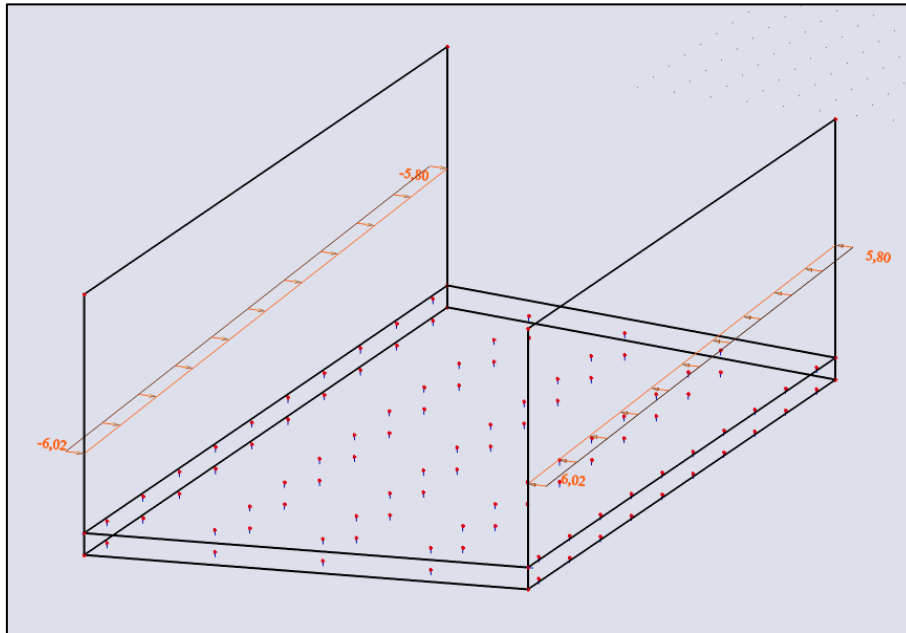
Figure 46: Clamping load

12.2.7   Horizontal traffic load

Figure 47 shows how the horizontal traffic load is placed in the model.
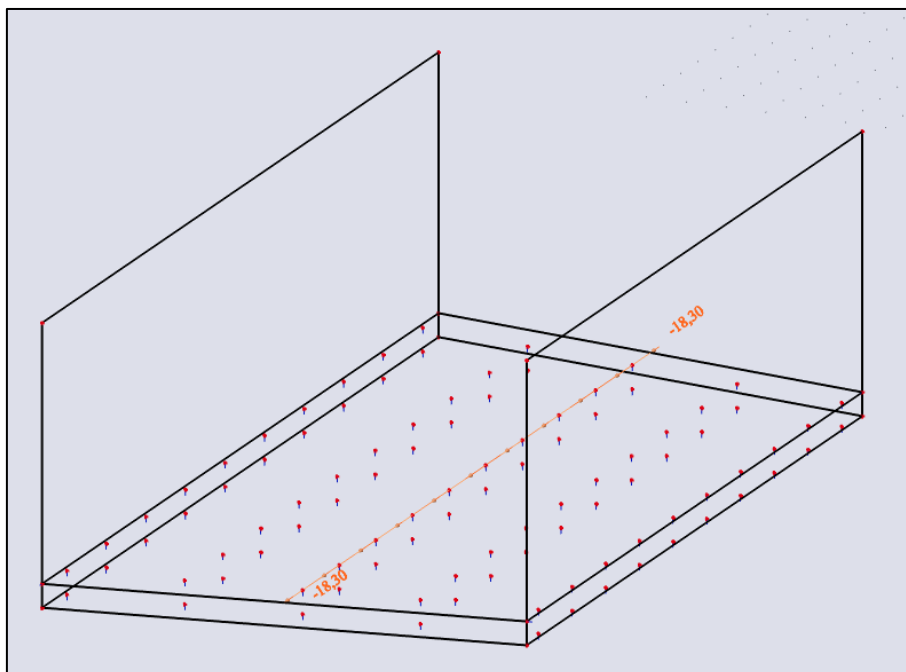
Figure 47: Horizontal traffic load (Braking)

12.2.8   Vertical traffic loads

Figure 48 and Figure 49 show how the vertical traffic loads are placed in the model.

Figure 48: Vertical traffic load (surface)

Figure 49: Vertical traffic load (concentrated/vehicle)

12.3 Results

12.3.1   First control perimeter u_1

Regular Floor

The figures below show the first control perimeters of layout A to D for the regular floor. The control perimeter for the internal columns for layout A, B, C, and D are 5.3 m, 8.4 m, 5.9 m and 5.3 m respectively.
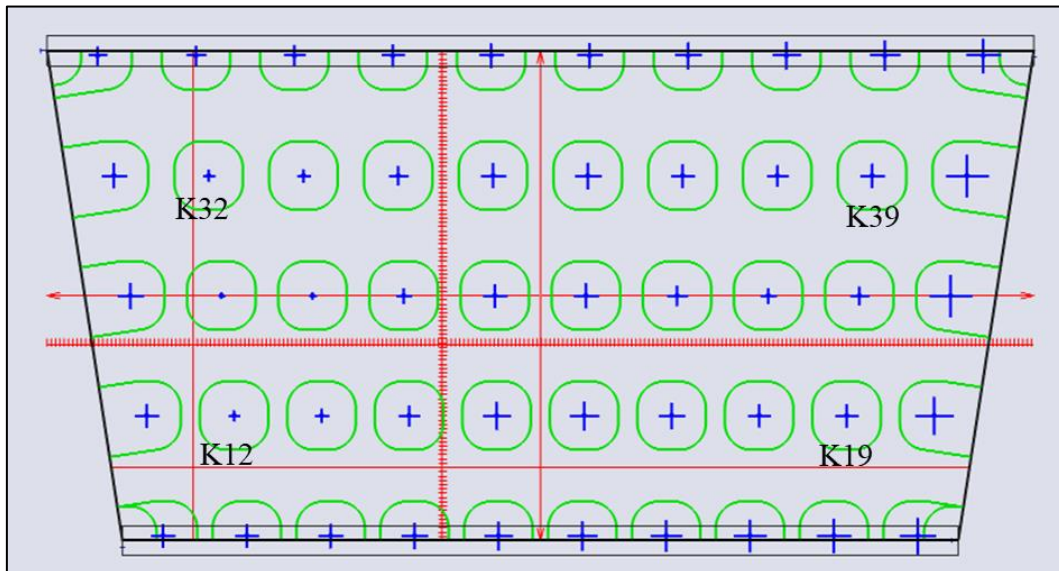
Figure 50: First control perimeter regular floor layout A
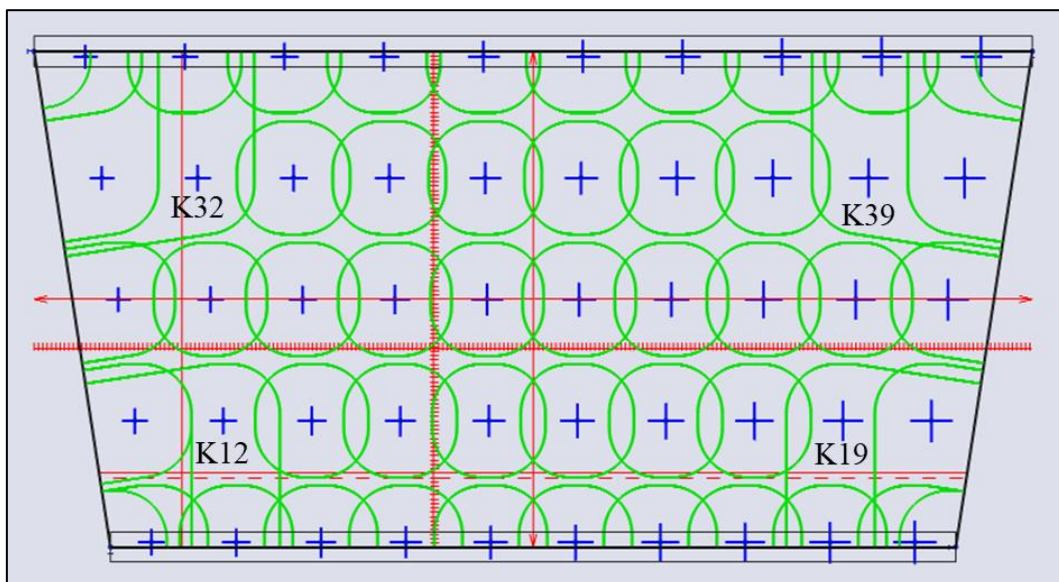
Figure 51: First control perimeter regular floor layout B

Layout B has 4 anchor points (K12,K19,K32 and K39) for which the first control perimeter deviates from the respective anchor points on the other layouts. As can be seen in Figure 51 the perimeter

connects to the outer edge making it from an internal column to a corner column. This is for a large amount the reason why the results show a higher stress levels at these locations for layout B.
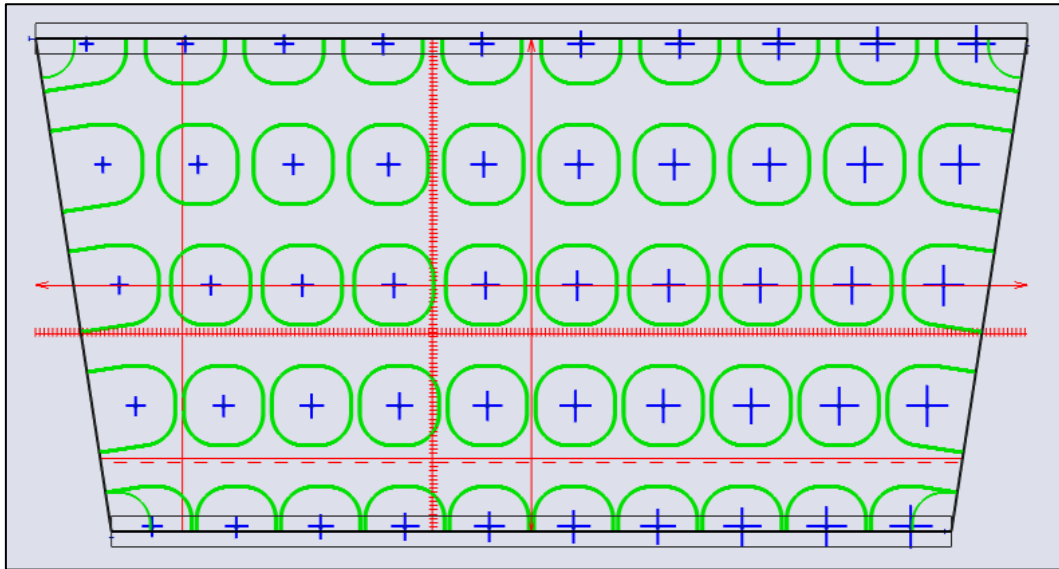
Figure 52: First control perimeter regular floor layout C
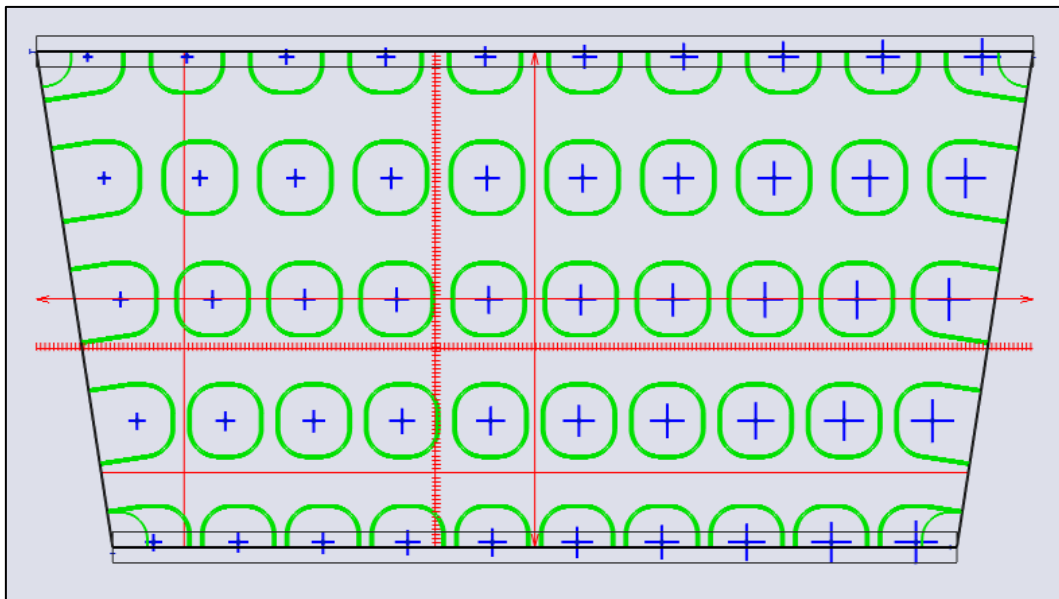
Figure 53: First control perimeter regular floor layout D

Underwater concrete Floor

Figure 54 to Figure 57 show the control perimeters for layout A to D for the underwater concrete floor. As these floors are thicker than the regular floor the perimeters differ to those of the regular floor. The length of the control perimeter amounts to 6.43 m, 9.71 m, 7.26 m and 6.66 m respectively. Also here the perimeters for anchor points K12, K19, K32 and K39 connect to the outer edge at layout B.
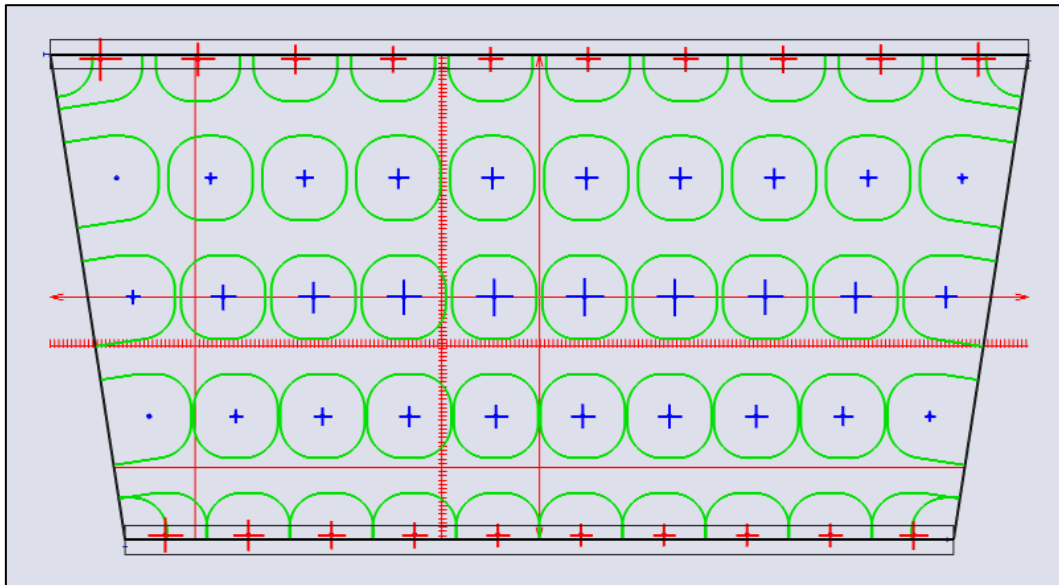
Figure 54: First control perimeter UWC floor layout A
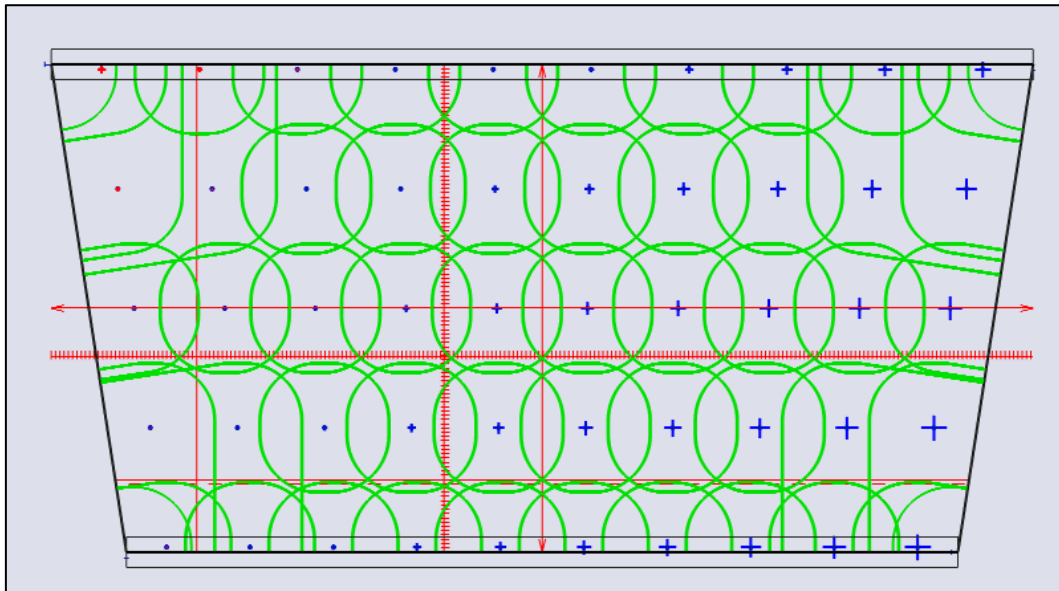
Figure 55: First control perimeter UWC floor layout B

Figure 56: First control perimeter UWC floor layout C

Figure 57: First control perimeter UWC floor layout D

12.3.2 Net Force Distribution

This chapter shows the net force distribution of the layouts at the six different cases. The blue arrows indicate the compressive forces the anchors have to absorb while the red arrows indicate the tensile forces that need to be absorbed. The size of the arrow indicates the magnitude of the force. The arrows are ordered from left to right respectively anchor K1 to K50.

Regular Floor

First for the regular floor at LowWaterSummer and HighWaterWinter load combinations respectively.
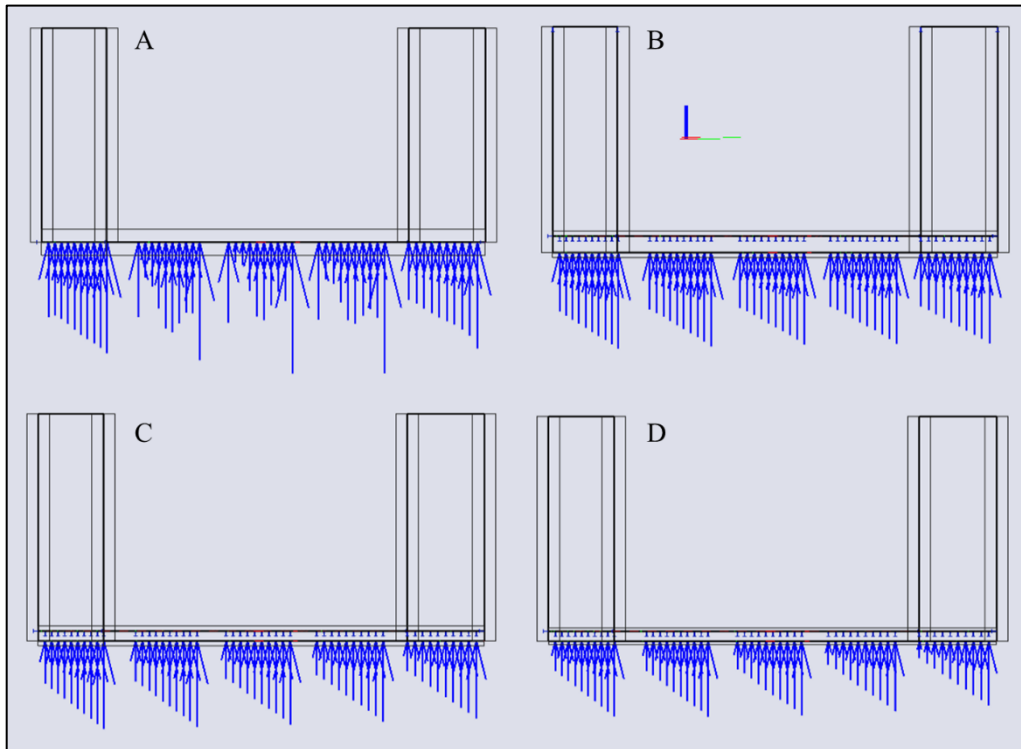
Figure 58: Net force distribution regular floor LowWaterSummer
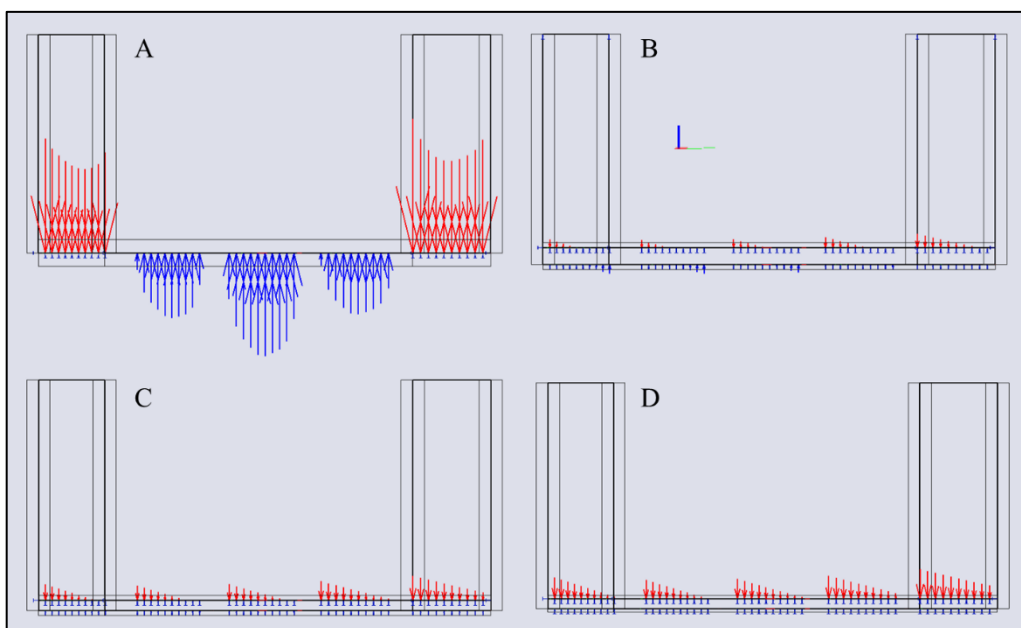
Figure 59: Net force distribution regular floor HighWaterWinter

UNIVERSITY
OF TWENTE.

anteagroup

Layout B to D show a gradual distribution for both load combinations. Being more compressive during LowWaterSummer and shifting more towards tension during HighWaterWinter. Layout A follows mostly a similar distribution at the first load combination but differs much at the second. Also the scale of the net force during HifhWaterWinter combination is drastically larger compared to Layout B-D.

Underwater concrete floor Initial

Figures Figure 60 and Figure 61 show the net force distributions for the underwater concrete floor during initial placement for LowWaterSummer and HighWaterWinter load combinations respectively.
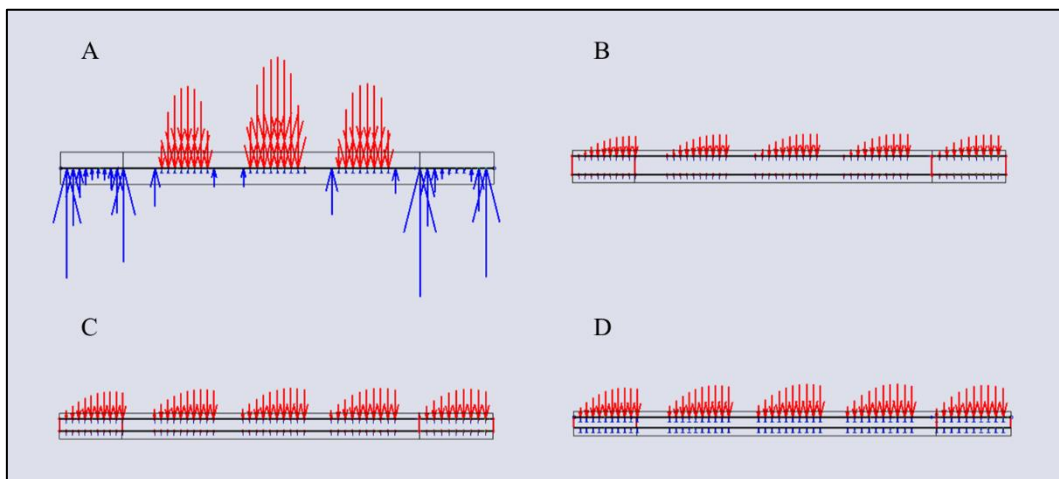
Figure 60: Net force distribution UWC floor initial placement LowWaterSummer
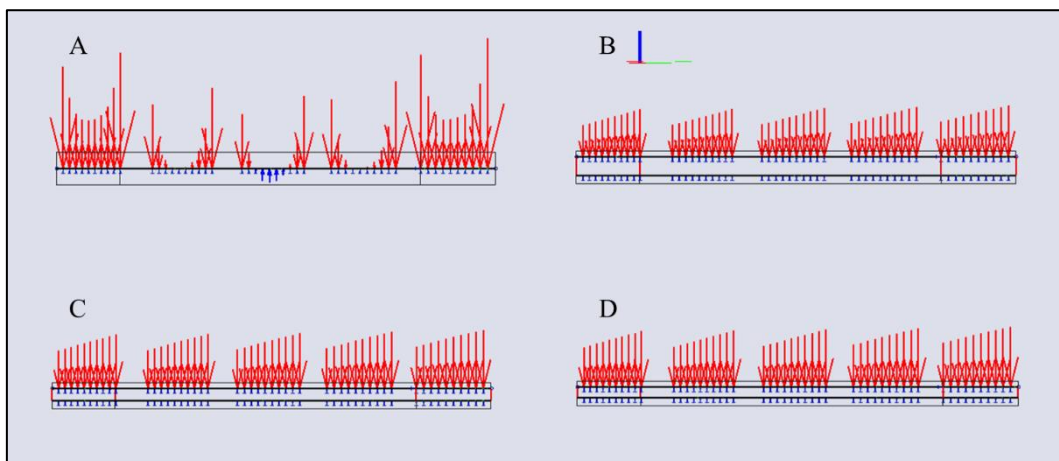
Figure 61: Net force distribution UWC floor initial placement HighWaterWinter

The results for Layout B-D have similar shapes to the previous figures now being more shifted towards tensile forces. Which is a direct result of lacking compressive forces otherwise exerted by the self-weight of the walls and traffic loads. Layout A displays odd force distributions with a lot of aberrations/ highs and lows.

Underwater concrete floor Final

Finally, Figure 62 and Figure 63 show the net force distributions for the underwater concrete floor during the final situation for LowWaterSummer and HighWaterWinter load combinations respectively.
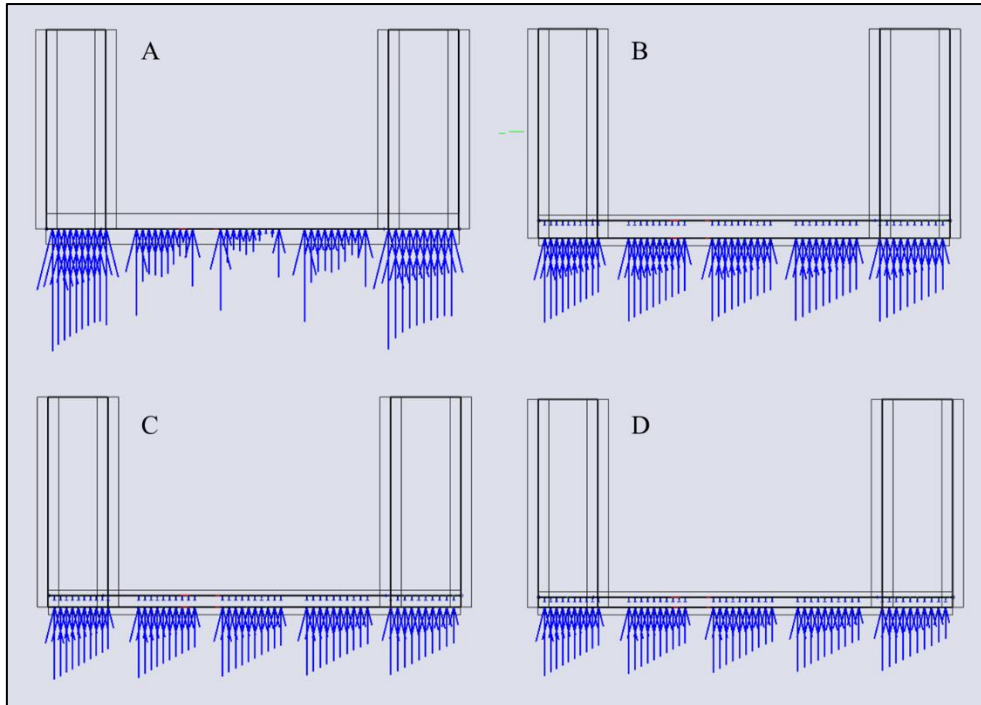
Figure 62: Net force distribution UWC floor final situation LowWaterSummer
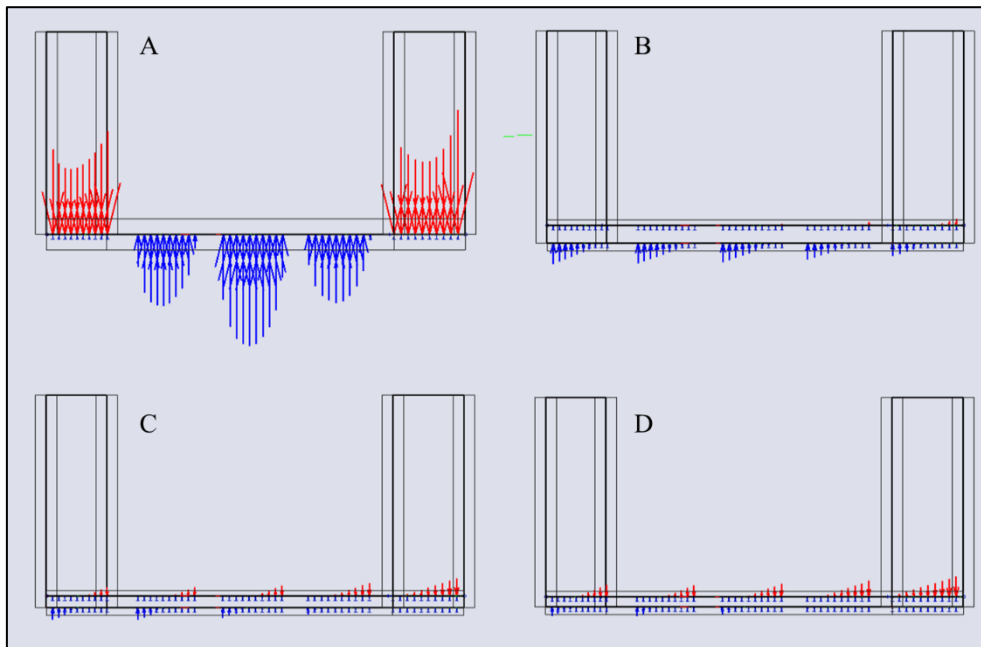
Figure 63: Net force distribution UWC floor final situation HighWaterWinter

The above figures show very comparable force distributions as for the regular floor. As the mere difference affecting the distribution between the two cases is a slightly thicker floor. Thus slightly higher compressive forces. This is nicely represented in the figures especially visible in Layout B-D during the HighWaterWinter combination.

12.3.3 Alternative diagrams

Some results for the underwater concrete floors deviated much from the other layouts, which made it difficult to notice the differences on lower scales. This chapter is devoted to adapted diagrams that exclude some of the peaks at edge columns. For layout A which was the source of these abnormal peaks, only the results for the internal columns will be shown or the layout will be entirely left out. The alternative diagrams are made for the cases highlighted in the table below.

Floor type	Load combination	Moment in time	Perimeter	Change
Underwater concrete floor	LowWaterSummer	Initial placement	U0	No peaks
			U1	No peaks
		Final situation	U0	-
			U1	-
	HighWaterWinter	Initial placement	U0	Left out entirely
			U1	Left out entirely
		Final situation	U0	No peaks
			U1	No peaks
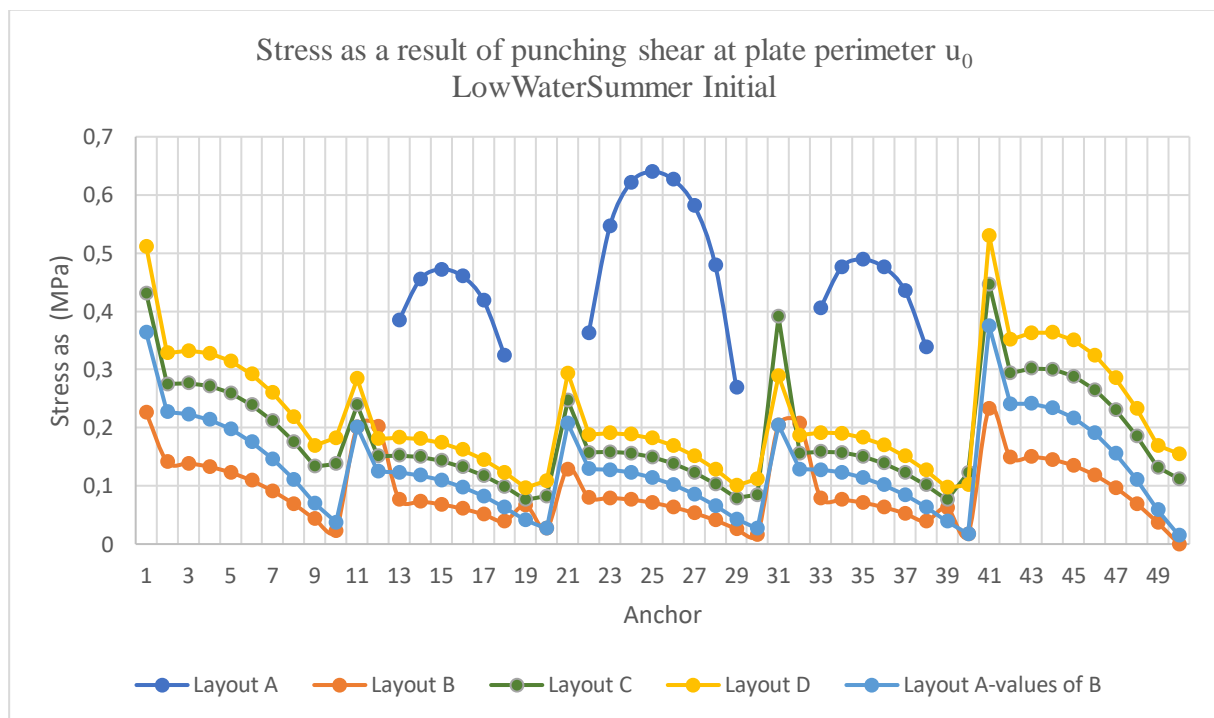
Figure 64: Stress Diagram UWC floor LowWaterSummer perimeter u0 initial excluding peaks
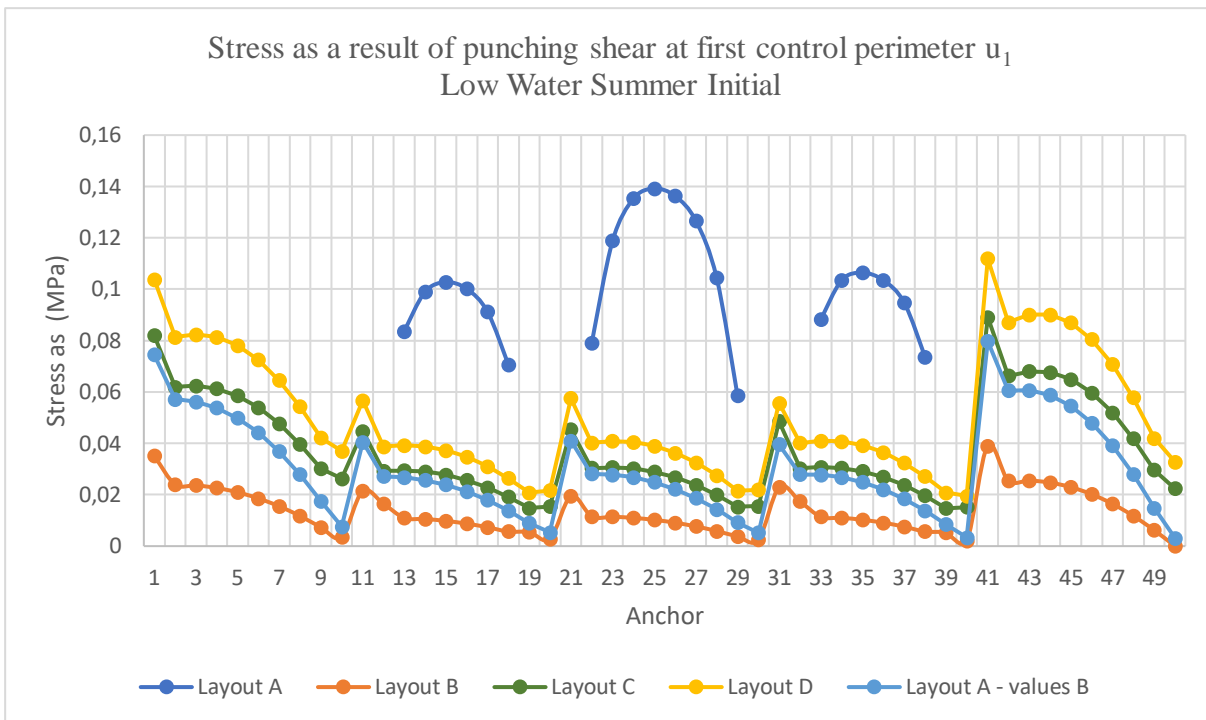
Figure 65: Stress Diagram UWC floor LowWaterSummer perimeter u1 initial excluding peaks
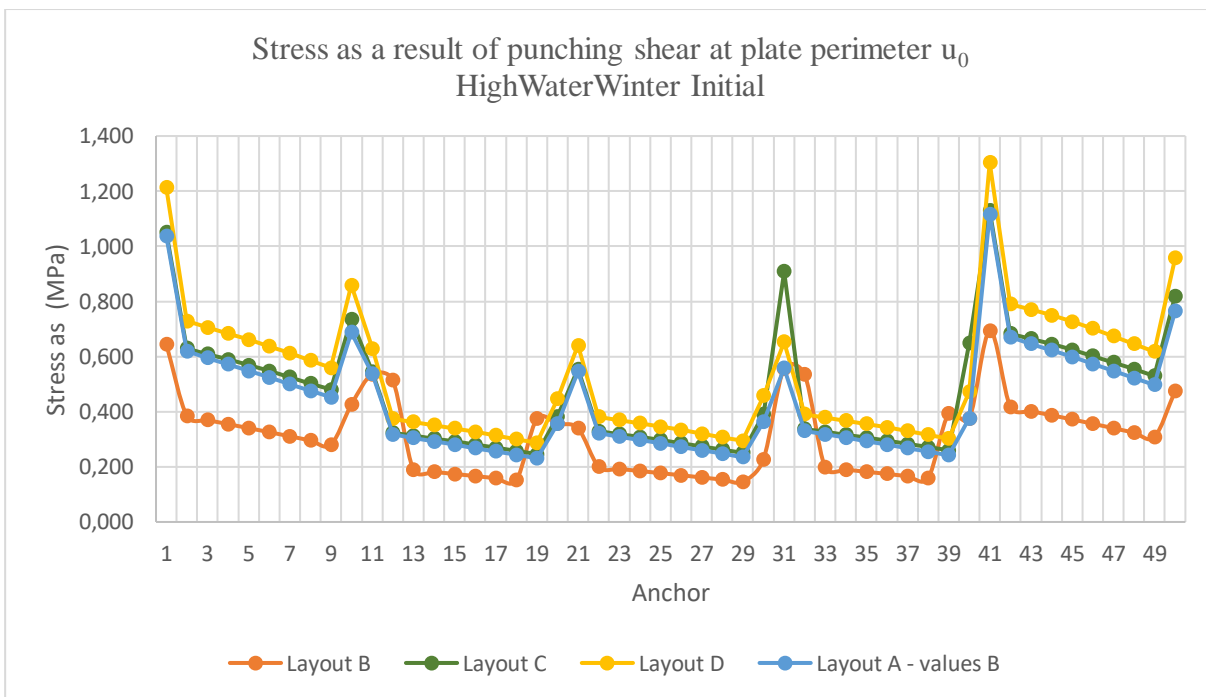
Figure 66: Stress Diagram UWC floor HighWaterWinter perimeter u0 initial excluding layout A

UNIVERSITY
OF TWENTE.

anteagroup
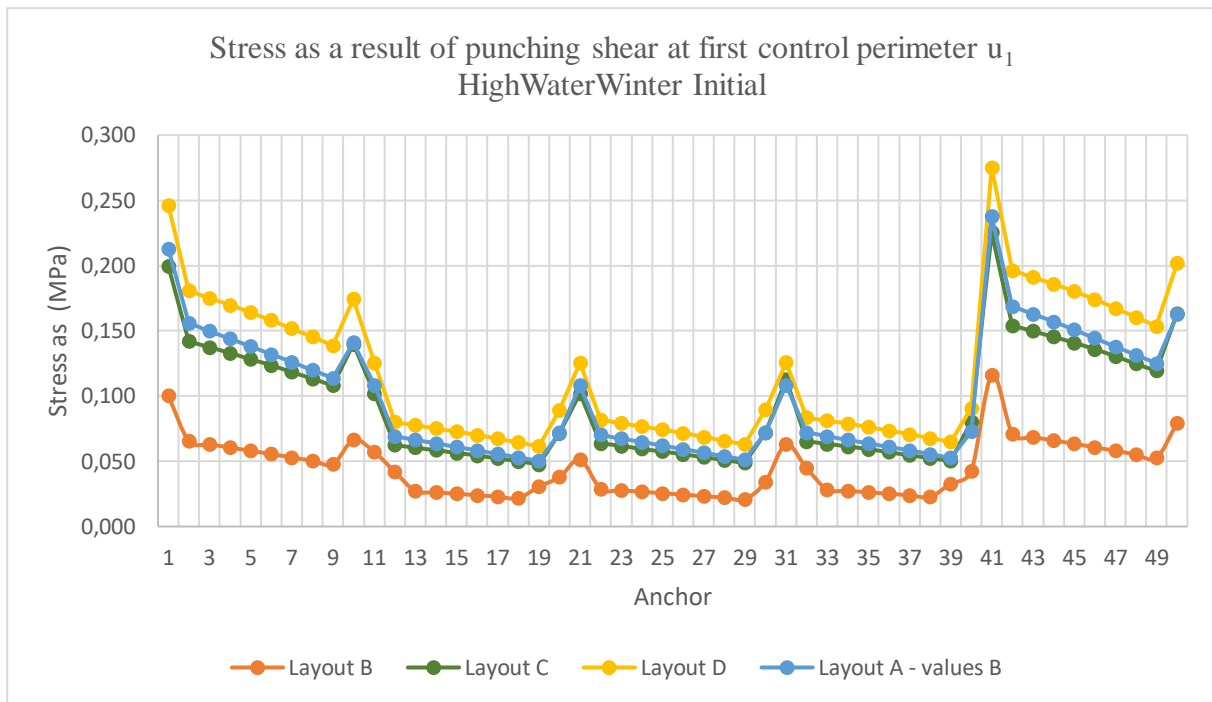
Figure 67: Stress Diagram UWC floor HighWaterWinter perimeter u1 initial excluding layout A
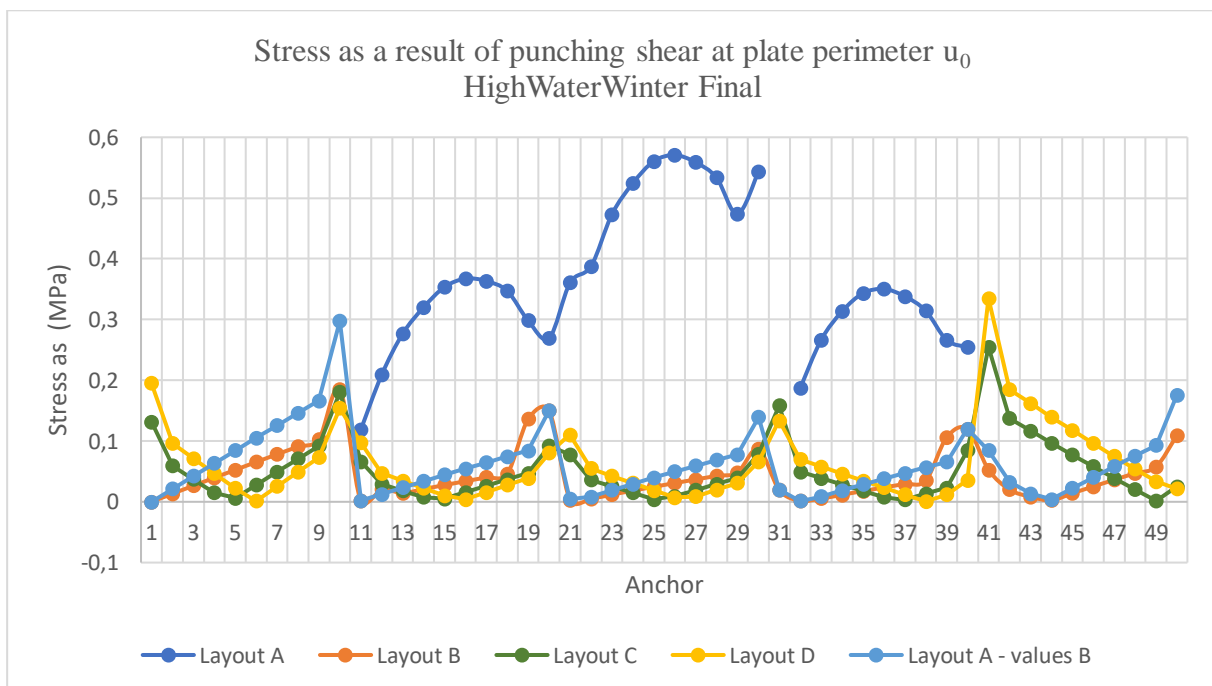
Figure 68: Stress Diagram UWC floor HighWaterWinter perimeter u0 final excluding layout A

UNIVERSITY
OF TWENTE.

anteagroup
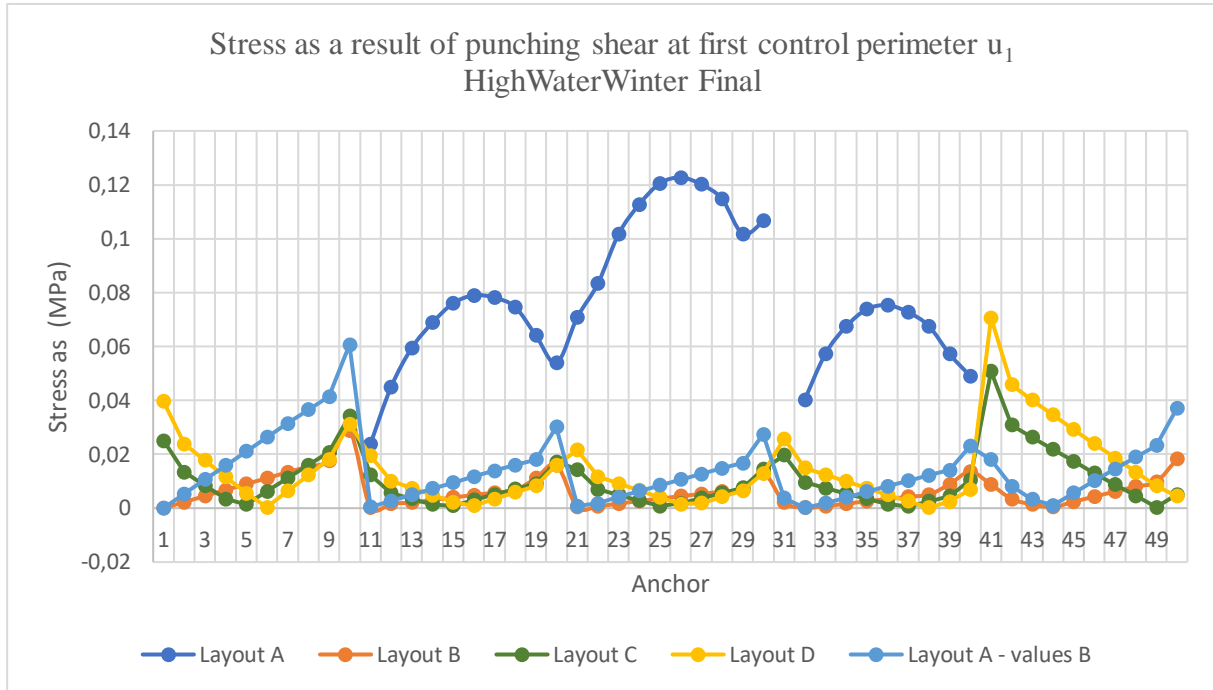
Figure 69: Stress Diagram UWC floor HighWaterWinter perimeter u1 final excluding layout A